Politecnico di Torino

Master's degree program in Civil Engineering

Use of Chromium Steel Sludge in Bituminous Mastics for Road Paving Applications

Tutors

Prof. Ezio Santagata

Dr. Sadegh Yeganeh

Candidate

Amir Jaleh

March 2026

Abstract

The road construction industry continuously explores the use of new alternative materials for asphalt pavements. At the same time, industrial activities generate massive amounts of by-products every year, such as chromium steel sludge from bearing manufacturing. This research aims to evaluate the feasibility of utilizing this chromium steel sludge as an alternative mineral filler in bituminous mastics. By incorporating this material into the bitumen matrix, the study investigates its potential to replace standard road fillers and its overall impact on mastic performance. To achieve this objective, the physical properties of the chromium sludge were first characterized and compared with two conventional reference fillers: a commercial filler (Rheofiller) and ordinary Portland cement. The evaluation included particle density determination using a pyknometer and void content analysis via the Rigden voids test. Subsequently, asphalt mastics were formulated using a 50/70 penetration grade neat bitumen at three distinct volumetric filler-to-binder (F/B) ratios (0.6, 1.0, and 1.4) to examine the influence of filler type and concentration. The rheological behavior of the prepared mastics was assessed in both unaged and long-term aged conditions, with the aging process simulated using a Pressure Aging Vessel (PAV). A Dynamic Shear Rheometer (DSR) was utilized to conduct frequency sweep tests, enabling the construction of complex shear modulus master curves to analyze the linear viscoelastic properties. Finally, the self-healing capability and fatigue life of the mastics were evaluated through advanced DSR testing. This was achieved by employing specific Fatigue-Rest-Fatigue (FRF) and Rest-Fatigue (RF) protocols to calculate the stiffness recovery index (IG) and the fatigue endurance index (IN).

Contents

List of Figures

List of Tables

List of Abbreviations

LVE	Linear Viscoelastic
NLVE	Non-Linear Viscoelastic
ZSV	Zero Shear Viscosity
RTFOT	Rolling Thin-Film Oven Test
PAV	Pressure Aging Vessel
NAAT	Nitrogen Atmosphere Oven Aging Test
BS	British Standards Institution
EN	European Norm
F/B	Filler to Bitumen
DSR	Dynamic Shear Rheometer
WLF	Williams-Landel-Ferry
FRF	Fatigue-Rest-Fatigue
RF	Rest-Fatigue
VMA	Voids in Mineral Aggregate

List of Symbols

t	the exact temperature of the water in °C
m_0	mass of the empty pyknometer in gram
m_1	mass of the pyknometer containing the dry filler in gram
m_2	mass of the pyknometer containing the filler and filled with the liquid in gram
m_3	mass of the pyknometer fully filled with water in gram
m_4	mass of the pyknometer fully filled with alcohol in gram
m_5	mass of the compacted filler in grams
P_w	density of the water in Mg/m3
V_p	volume of the pyknometer in milliliters
$P_{alcohol}$	density of the alcohol in Mg/m3
P_f	particle density of the specific filler in Mg/m3
V_r	void content expressed as a percentage
a	inner diameter of the dropping block cylinder in millimeters
h	height of the compressed filler in millimeters
$G^*(\omega_r)$	complex shear modulus at the reduced angular frequency
G_g	glassy shear modulus of the material
ω_r	reduced angular frequency
ω_0	characteristic angular frequency
R	rheological index
a_T	time-temperature shift factor
ω	actual angular frequency at the test temperature

T	specific test temperature in °C
T_{ref}	standard reference temperature in °C
C_1	empirical constants
C_2	empirical constants
$\Delta\lvert G^*\rvert_{R-\mathrm{FRF}}$	Difference of complex modulus in rest part in FRF test
$\Delta\lvert G^*\rvert_{R-\mathrm{RF}}$	Difference of complex modulus in rest part in RF test
$\Delta\lvert G^*\rvert_{\mathrm{F}-\mathrm{FRF}}$	Difference of complex modulus in fatigue part in FRF test
$\mathrm{N_{FRF}}$	Number of cycles until 35% reduction in $\mathrm{G^*}$ in FRF test
$\mathrm{N_{RF}}$	Number of cycles until 35% reduction in $\mathrm{G^*}$ in RF test

Chapter 1: Introduction

1.1 General Perspective

Road networks are a basic part of modern life. They connect cities, support the economy, and make daily travel possible. Building and maintaining these roads requires a massive amount of construction materials. Since pavements constantly face heavy traffic loads and changing weather conditions, choosing the right materials is very important to make sure the roads last a long time.

Most roads today are built using flexible pavements, which are primarily made of asphalt mixtures. Asphalt is a combination of stone aggregates and a binder, which is usually bitumen. However, inside this mixture, the bitumen does not just act alone. It mixes with very fine mineral particles, known as fillers, to create a blend called asphalt mastic. This mastic acts as the true "glue" that coats and holds all the bigger stones together. The overall strength, durability, and lifespan of the road depend heavily on how this mastic behaves (Chen et al., 2019).

These days, standard mineral fillers or ordinary Portland cement are used for this job in the paving industry. The specific type and amount of filler control how the mastic reacts to hot and cold temperatures (Zheng et al., 2018). Because the mastic directly controls how the asphalt handles everyday stress (J. Hou et al., 2022), studying and picking the right filler is one of the most important parts of pavement engineering. In this study, a new industrial by-product is introduced and evaluated as a potential alternative to these traditional fillers.

1.2 Problem Statement

Industrial activities generate a significant amount of waste each year. One notable example is chromium steel sludge, an industrial by-product produced during bearing manufacturing. The reuse of such by-products in different industries can provide both environmental and economic benefits. One potential application of this material is its use as a filler in asphalt mixtures. However, this possibility must be evaluated through laboratory investigations to assess its feasibility, as well as its potential advantages and limitations.

In this study, the investigation begins at the mastic level, which consists of the binder and filler without the presence of aggregates. This approach allows for a more fundamental understanding of the interaction between chromium steel sludge and the bitumen. By isolating these components, it becomes easier to evaluate the effects of the filler on the rheological and mechanical properties of the material before moving to more complex asphalt mixtures.

1.3 Research Objectives and Thesis Outline

The main goal of this research is to evaluate chromium steel sludge as a sustainable alternative filler in asphalt mastics. To reach this goal, a few specific objectives were established. First, the physical properties of the chromium sludge need to be compared with standard materials like Rheofiller and Portland cement. Next, an assessment is made to understand how the type of filler and the amount of filler, known as the filler-to-binder ratio, change the stiffness and overall behavior of the mastic. After that, the different mastics are tested to see how they age over time using a Pressure Aging Vessel. Finally, the self-healing ability and fatigue life of the mastics are measured to find out if the chromium sludge improves or degrades the material's ability to recover from damage.

To cover all these points clearly, this thesis is organized into five main chapters. Chapter 1 introduces the general background, the problem with industrial waste, and the goals of the study. Following this, Chapter 2 provides the background and literature review. It explains the basics of asphalt mastics, their rheological behavior under stress, how the aging mechanism works, and the science behind the healing mechanism in bitumen.

Chapter 3 then details the materials and methods. It explains the properties of the neat bitumen and the three types of fillers, and shows how the mastics were prepared. It also breaks down the

laboratory testing methods, including filler characterization, frequency sweep tests, and the specific healing test protocols. Following the methodology, Chapter 4 presents all the laboratory results. This chapter shows the initial characterization of the materials and explains the exact effect of the filler type and ratio on the mastic before aging, after aging, and during the self-healing process. Finally, conclusions are presented in Chapter 5. It summarizes the most important findings and gives a clear answer on whether chromium steel sludge is a practical and useful alternative material.

Chapter 2: Background and Literature Review

2.1 Introduction to Asphalt Mastic

Asphalt mixtures are widely used in pavement construction, and within this structural system, asphalt mastic is considered a key component. The performance and service life of asphalt mixtures are strongly influenced by the behavior of this phase. Asphalt mastic consists of a combination of asphalt binder and fine mineral filler. Since the stiffness of the filler is typically much higher than that of the binder, it acts as a reinforcing material within the system (Tan & Guo, 2013).

To better quantify this influence, Bi et al. (2021) investigated the relationship between mastic properties and the dynamic modulus of asphalt mixtures. Their results showed that the dynamic modulus master curve of the mixture is primarily affected by the binder type and the filler-to-binder ratio, while the specific type of filler has a comparatively smaller effect. Moreover, a strong correlation was observed between the complex shear modulus of the mastic and the dynamic modulus of the final mixture. These findings demonstrate that evaluating mastic properties can provide a reliable prediction of the macroscopic performance of asphalt mixtures and highlight the importance of optimizing the filler-to-binder ratio.

Furthermore, asphalt mixtures can be conceptualized as a three-phase system composed of a coarse aggregate skeleton, asphalt mastic, and air voids (X. Li et al., 2026). In this framework, the mastic acts as the binding medium that holds the aggregate structure together. Therefore, its composition and properties directly control the mechanical performance and long-term durability of the pavement. This underscores the importance of carefully evaluating alternative filler materials, as their interaction with the binder ultimately governs the behavior of the entire mixture under traffic and environmental loading.

2.2 Rheological Behavior of Asphalt

Asphalt mastic, the critical binding matrix within flexible pavements, demonstrates complex viscoelastic behavior that is fundamentally governed by the interaction between the bituminous binder and mineral fillers. The addition of solid filler particles alters the inherent rheological response of the base binder, generally resulting in a pronounced stiffening effect. Research demonstrates that the inclusion of mineral fillers increases the complex shear modulus (G^*) and decreases the phase angle, effectively shifting the material's behavior toward a more elastic response under dynamic loading (Chen et al., 2019; Y.-R. Kim & Little, 2004). This stiffening mechanism is primarily attributed to a combination of volume-filling effects and physicochemical interactions at the binder-filler interface, which physically restrict the mobility of the bitumen molecular chains.

The altered rheological properties directly influence the macroscopic performance of the pavement, particularly its susceptibility to temperature-induced distresses like permanent deformation. At elevated temperatures, the presence of mineral fillers significantly enhances the rutting resistance of the mastic matrix. Studies focused on high-temperature rheological behavior have shown that optimizing the filler content increases critical performance indicators, such as the rutting parameter ($G^*/\sin\delta$), providing essential structural stability under repeated traffic stresses (S. Li et al., 2021). However, a careful balance must be maintained; while higher filler concentrations improve high-temperature stability, an overly stiff matrix can become excessively brittle, potentially compromising the material's resistance to low-temperature thermal cracking and fatigue (Chen et al., 2019)

To accurately characterize these complex stress-strain relationships across various environmental conditions, rheological evaluations of asphalt mastics are typically conducted within the linear viscoelastic (LVE) domain using a Dynamic Shear Rheometer (DSR). Advanced LVE analysis allows researchers to construct master curves of the complex modulus and relaxation modulus over a wide range of frequencies and temperatures (Y.-R. Kim & Little, 2004; Yeganeh et al., 2020). Furthermore, evaluating the direct relationship between the unaged base binder and the resulting mastic is essential for advanced mix design. Experimental testing indicates that reliable predictive relationships can be established to estimate a mastic's rheological performance based on the

specific characteristics of the base binder and the volumetric fraction of the filler incorporated (Riccardi et al., 2018).

Beyond simple mechanical reinforcement, the specific geometric characteristics, porosity, and mineralogy of the filler deeply influence the internal microstructure of the mastic. The physical interaction between the solid particles and the asphalt binder dictates the proportion of "fixed bitumen" - the binder absorbed into the filler's surface and internal voids - versus the remaining "free bitumen," which provides necessary lubrication and flowability. Understanding this fundamental interaction mechanism is vital, as the effective combined volume of the rigid phase (the solid filler plus the fixed bitumen) strongly governs the zero-shear viscosity, shear-thinning behavior, and the overall long-term durability of the mastic under traffic loading (Chen et al., 2019).

To fully grasp how mastics perform, it is important to briefly review the basics of binder rheology. The rheological evaluation of asphalt materials involves analyzing their behavior across both the linear viscoelastic (LVE) and nonlinear viscoelastic (NLVE) domains. Fundamentally, this characterization relies on measuring the storage modulus, which represents the elastic (in-phase) component of the stress-strain response, and the loss modulus, which defines the viscous (out-of-phase) component. As outlined by Salehfard et al., (2024), the LVE behavior of these materials is often characterized using parameters such as the rheological index—a shape parameter associated with the width of the relaxation spectrum—and the zero shear viscosity (ZSV). The ZSV, calculated when the shear rate approaches zero, serves as a vital indicator of the material's inherent stiffness and its resistance to permanent deformation. Furthermore, while testing at low stress levels captures the undamaged LVE properties, understanding the nonlinear response under heavier stresses is equally critical, as actual pavement distresses like rutting cannot be fully explained by linear viscoelastic phenomena alone.

2.3 Aging of Asphalt Mastic

The long-term performance of flexible pavements is heavily affected by the aging of the asphalt mixture. This aging process is primarily driven by the oxidation of the bitumen when it is exposed to air and temperature changes over time. However, the aging behavior is significantly altered when mineral fillers are mixed with the bitumen to form a mastic. In a detailed study by Wu &

Airey, 2011, the specific influence of mineral fillers on the aging properties of mastics was investigated. It was demonstrated that the inclusion of fillers generally reduces the aging susceptibility of the base binder. When the solid filler particles are dispersed within the bitumen, a physical barrier is created. This barrier effectively restricts the diffusion of oxygen into the mastic, which slows down the overall oxidative reactions.

Furthermore, it was concluded by them that the physical and chemical characteristics of the filler, such as its specific surface area and volume concentration, heavily dictate the extent of this protective effect. Because the filler particles interact directly with the binder, the long-term durability of the pavement is highly dependent on the chosen filler. These findings make it clear that any new alternative material must be carefully evaluated under accelerated aging conditions

To fully understand how bituminous materials degrade over their service life, it is essential to explore the underlying physicochemical phenomena that govern binder aging. Fundamentally, aging is driven by the oxidation of the binder and the continuous evaporation of its lighter volatile components. From a chemical perspective, these reactions lead to a measurable increase in highly polar functional groups, specifically carbonyls and sulfoxides, which form progressively as the material undergoes long-term oxidative aging. Beyond these chemical shifts, aging induces profound physical and microstructural transformations within the matrix. As microscopic analyses (such as Atomic Force Microscopy) have demonstrated, the aging process triggers a phase transition where the lighter, more oily maltene fractions gradually transform into heavier, complex asphaltene molecules. This microstructural reorganization is physically characterized by an increase in surface roughness and the prominent growth of "bee-shaped" asphaltene structures. Ultimately, this combined physicochemical evolution results in the gradual hardening of the asphalt, significantly increasing its viscosity, reducing its ductility, and making the overall pavement highly susceptible to low-temperature cracking and fatigue.(Dadaei et al., 2024)

To accurately predict long-term pavement performance, it is crucial to simulate the aging process of bituminous materials in the laboratory. Conventionally, this simulation is divided into two phases: short-term aging, which replicates the high-temperature degradation during mixture production using the Rolling Thin-Film Oven Test (RTFOT), and long-term aging, which simulates in-service environmental exposure using the Pressure Aging Vessel (PAV). These standardized procedures utilize elevated temperatures and pressures to accelerate the thermal-oxidative aging

rate. However, recent experimental approaches aim to better decouple the distinct mechanisms of aging. To isolate the individual effects of heat and oxygen on bituminous binders, thin-film aging tests can be conducted under varying atmospheric conditions, such as ambient air versus an inert nitrogen environment. When the material is subjected to elevated temperatures in the absence of oxygen, it does not exhibit significant stiffening. this indicates that while standard thermal conditioning inevitably leads to the volatilization of lighter chemical fractions, the severe physical hardening of the bituminous matrix is predominantly governed by oxidative aging (Camargo et al., 2020).

While the standard aging protocol relies on a two-step process - utilizing the RTFOT to simulate short-term aging followed by a 20-hour PAV procedure for long-term aging - researchers have explored more streamlined approaches. Notably, a comparative study by Migliori & Corté, (1998) investigated whether the initial short-term aging step could be bypassed entirely by extending the duration of the pressure vessel conditioning. Through extensive rheological and conventional consistency testing, they demonstrated a direct equivalence between the standard combined procedure (RTFOT followed by 20 hours of PAV) and a simplified, continuous 25-hour PAV aging process conducted at 100°C and 2.1 MPa. For the unmodified binders investigated, bypassing the RTFOT and directly subjecting the material to 25 hours of PAV yielded comparable physical and low-temperature rheological degradation. This alternative provides a highly efficient and simplified laboratory methodology for simulating the total life-cycle aging of bituminous materials.

In exploring the aging behavior of bituminous mastics, recent literature emphasizes that the physical and chemical characteristics of the specific filler type are critical to the material's durability. As highlighted by Xie et al., (2020) , a filler's specific mineralogy, particle size, and porosity fundamentally alter the aging trajectory of the binder. For instance, comparative studies note that highly porous materials, such as diatomite, perform significantly better than standard mineral powders in hindering thermal oxidative aging due to their unique micropore structures. Furthermore, Xie et al. emphasize that the aging resistance is heavily influenced by the chemical composition of the filler (such as its SiO_2 content), which directly dictates the absorption capacity and the resulting proportion of "structural asphalt" formed at the binder-filler interface. Beyond these chemical and structural interactions, the sheer physical presence of the mineral filler acts as

a barrier that shields the matrix from severe ultraviolet degradation, effectively reducing the mastic's temperature susceptibility and aging-induced fatigue. Therefore, when evaluating a novel alternative material like chromium steel sludge, it is essential to consider how its specific mineralogical profile and porosity will compare to traditional filler types in protecting the binder from both thermal and photo-oxidative aging.

2.4 Healing Mechanism

Another critical property of asphalt materials is their inherent ability to self-heal. During rest periods, when traffic loads are temporarily removed, bituminous binders can naturally close micro-cracks and recover a portion of their original structural strength. This healing mechanism is highly dependent on both the duration of the rest period and the environmental temperature (Santagata et al., 2022). However, accurately evaluating this property in the laboratory presents a significant challenge. During a rest period, the stiffness of the binder can artificially increase due to reversible, time-dependent physicochemical phenomena - such as steric hardening - which are entirely unrelated to actual damage repair (Santagata et al., 2022).

To isolate true structural recovery from simple temporary hardening, specialized testing protocols are required. Recent methodologies employ a combination of Fatigue (FRF) and Rest-Fatigue (RF) testing. By comparing the results of a continuous fatigue test with one that incorporates a scheduled rest period, researchers can accurately quantify the exact amount of stiffness recovery and the subsequent gain in fatigue endurance caused solely by the healing of micro-cracks. Through the establishment of specific healing indices, this methodology provides a robust framework for evaluating the true healing potential of mastics modified with new alternative fillers (Miglietta et al., 2021; Santagata et al., 2022).

The specific characteristics of mineral fillers fundamentally govern the actual healing capability of the material within the pavement. While the self-healing process is driven primarily by the elastic recovery, viscous flow, and molecular diffusion of the binder, the physical presence of filler particles alters the thermodynamics of the matrix. Specifically, the morphological and geometric properties of a filler directly dictate the temperature threshold required to initiate self-healing. Industrial by-products, such as steel slag, possess a significantly coarser surface texture and superior geometric characteristics compared to conventional limestone. This unique morphology

fosters a stronger interaction within the bitumen matrix, allowing the mastic to achieve a near-Newtonian flow state more rapidly. Consequently, mastics formulated with steel slag initiate the crack-closure process at measurably lower temperatures than those using traditional fillers (C. Li et al., 2018). This suggests that integrating structurally similar alternative materials, such as chromium steel sludge, could potentially optimize flow behavior and significantly enhance the overall self-healing efficiency of the asphalt mastic.

Furthermore, the physicochemical phenomenon of self-healing is fundamentally understood as the reparation of a material's chemical structure to decelerate micro-fatigue damage (Xu et al., 2018). This healing mechanism is deeply tied to the specific composition and physicochemical characteristics of the bitumen and asphalt mixes (Williams, et al., 2001). At its core, the healing process is driven by molecular interactions within the asphalt. For instance, the healing rate of different asphalt mixtures is directly related to the molecular characteristics of their respective binders, pointing specifically to the importance of the methyl hydrogen-to-carbon ratio and the methylene-to-methyl group ratio (Kim et al., 1990).

To further explain these physicochemical interactions at the micro-level, Xu et al. (2018) note the advancement of molecular simulation and thermodynamic modeling. They reference Bhasin et al., (2011), who utilized molecular simulation techniques to explore how the chain length and chain branching of binder molecules correlate with their self-diffusivity, thereby expanding our understanding of how molecular architecture dictates self-healing properties. Additionally, Y. Hou et al., (2015), who developed a phase–field model that combined thermodynamic and mechanical approaches to provide a more comprehensive explanation of the physicochemical mechanisms driving crack closure and structural recovery in asphalt.

Chapter 3: Materials and Methodology

3.1 Materials

A neat bitumen with a penetration grade of 50/70 was selected as the base binder for all the mastics produced in this study. The binder was commercially supplied by Italiana Petroli S.p.A. and its physical and empirical properties comply with the European standard EN 12591, (2009). The detailed technical specifications provided from the producer and related standard requirements of the selected base bitumen are summarized in Table 1.

Table 1 – Characteristics of the bitumen (50/70)

Characteristic	Min. Limit	Max. Limit	Unit	Test Method
Penetration at 25°C	50	70	0.1 mm	EN 1426
Softening point	46	54	°C	EN 1427
Solubility	99	-	% weight	12592 EN
Flash point (Cleveland)	230	-	°C	2592 EN ISO
Relative density at 25/25°C	1000	1100	kg/m³	3838 EN ISO
Penetration Index	1.5	0.7	-	Annex A-12591 EN
:Resistance to hardening (RTFOT)				1-12607 EN
mass (Absolute value) Change in -	-	0.5	% weight	
penetration at 25°C Retained -	50	-	%	EN 1426
in softening point Increase -	-	11	°C	EN 1427

To establish a reliable baseline for evaluating the mastics, a standard commercial filler known as Rheofiller was utilized as the primary reference material. Rheofiller is a calcareous mineral filler obtained from the controlled grinding of carbonate rocks. It is widely utilized in the paving industry to complete the aggregate grading curve in the production of bituminous mixtures. Structurally, this specific filler is chemically inert and is guaranteed to be free from clayey materials, amorphous

silica, and organic matter. The technical and chemical properties of the Rheofiller, which conform to the European UNI (EN 13043, 2002) standard, are summarized in Table 2.

Table 2 – Characteristics of Rheofiller

Property	Value	Unit	Test Standard
Appearance	Grey powder	-	-
Passing 2.000 mm	100	%	UNI EN 933-10
Passing 0.125 mm	90 - 98	%	UNI EN 933-10
Passing 0.063 mm	78 - 88	%	UNI EN 933-10
Blaine Specific Surface Area	6000 - 7400	Cm^2/g	UNI EN 196-6
Particle Density	2.70 ± 0.05	Mg/m^3	UNI EN 1097-7
Calcium Carbonate Content	> 75	%	UNI EN 196-21
Chlorides Content	< 0.01	%	UNI EN 1744-1
Water Content	< 0.5	%	UNI EN 1097-5
Rigden Voids	$V_{28/39}$	-	UNI EN 1097-4
Increase in Softening Point (Ring & Ball)	$\Delta_{R\&B}8/16$	°C	UNI EN 13179-1
Bitumen Number	$BN_{28/39}$	-	UNI EN 13179-2
Water Solubility	WS_{10}	-	UNI EN 1744-1
Water Sensitivity	Not sensitive	-	UNI EN 1744-4
Methylene Blue Value	MBF_{10}	-	UNI EN 933-9
Release of dangerous substances	None	-	-

Following the Rheofiller, ordinary Portland cement was selected as the secondary reference filler to provide a baseline representative of common industry practices. The specific material utilized is a Portland limestone cement, classified as CEM II/B-LL 32.5 R, which is commercially produced by Colacem S.p.A. This product complies with the harmonized European standard (EN 197-1, 2011) and is certified for the preparation of concrete, mortar, and other construction mixtures.

Finally, chromium steel sludge was introduced as the primary material of interest in this research to evaluate its potential as a sustainable filler substitute. This industrial by-product is generated during the manufacturing and machining of steel components, particularly the production of bearings used in the automotive industry. To ensure its viability for reuse in road paving, a comprehensive chemical and physical characterization was provided by the producer.

The laboratory analysis confirmed that the sludge has a high solid content, with a dry residue of 97% at 105°C, making it a shovelable material. Environmentally, as stated in the chemical

composition analysis report, the sludge is classified under the European Waste Catalogue code 120115 as a non-hazardous waste, meeting toxicity limits for recovery applications. Chemically, the material is heavily metallic, composed primarily of iron (50%), alongside significant concentrations of chromium, manganese, and other trace metals and oxides. The key chemical constituents and physical properties of the chromium steel sludge are detailed in Table 3.

Table 3 – Chemical composition and physical properties of Chromium Steel Sludge

Property	Value	Unit	Test Standard
Physical State	Shovelable sludge	-	UNI 10802:2013
Dry Residue at 105°C	97	%	UNI EN 14346:2007 Met. A
Iron	50	%	UNI EN 13657:2004 + UNI EN 17294-2:2016
Chromium	5700	mg/kg	UNI EN 13657:2004 + UNI EN 17294-2:2016
Manganese	2300	mg/kg	UNI EN 13657:2004 + UNI EN 17294-2:2016
Copper	760	mg/kg	UNI EN 13657:2004 + UNI EN 17294-2:2016
Nickel	710	mg/kg	UNI EN 13657:2004 + UNI EN 17294-2:2016
Zinc	185	mg/kg	UNI EN 13657:2004 + UNI EN 17294-2:2016
Aluminum Oxide (Al_2O_3)	960	mg/kg	UNI EN 13657:2004 + UNI EN 17294-2:2016
Calcium (expressed as oxide)	640	mg/kg	UNI EN 13657:2004 + UNI EN 17294-2:2016
Silicon Oxide (SiO_2)	420	mg/kg	UNI EN 13657:2004 + UNI EN 17294-2:2016
Hydrocarbons (C10-C40)	3100	mg/kg	UNI EN 14039:2005
Total Organic Carbon (TOC)	1.5	%	UNI EN 13137:2002

The physical appearance of the three fillers evaluated in this study is shown in Figure 1. After the drying process was completed, all the materials were transformed into fine, loose powders. This preparation step was required so that the materials could be easily passed through sieves to accurately measure their particle sizes. Distinct colors were visually observed for each material. A whitish-gray color was shown by the Rheofiller, while a standard light gray color was displayed by the cement. In contrast, a much darker color, ranging from deep gray to almost black, was observed for the chromium steel sludge. Furthermore, the condition of the materials before they were dried was also recorded. Large clumps were heavily formed by the Rheofiller and the chromium steel sludge because their moist particles stuck together easily. On the other hand, very little clumping was observed in the cement, as their particles were kept relatively separate even before drying.

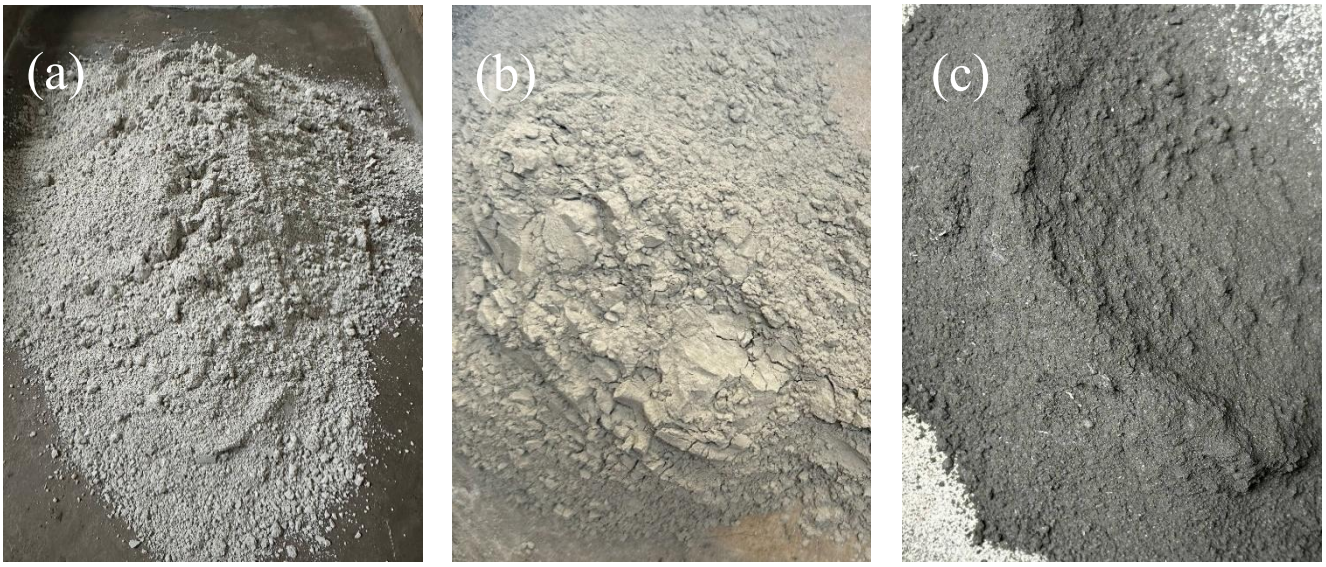

Figure 1 – Physical appearance of different fillers, a) Rheofiller b) Cement c) Chromium Steel Sludge

3.2 Filler Characterization

3.2.1 Particle Size Distributions

To ensure consistency and remove any trapped moisture, specific preparation protocols were followed for these materials. Both the cement and the Rheofiller were placed in an oven and dried at 110°C until a constant mass was successfully achieved. For the chromium sludge, an initial drying attempt was made at 150°C. However, due to a color change, likely caused by oxidation at this high temperature, a new sample of the sludge was prepared and dried at 110°C to prevent any compositional changes.

Following the drying process, all fillers were carefully sieved to obtain the specific material fraction passing through a 125 µm mesh. While the standard fillers passed through easily, the mechanical vibration process had to be repeated three times, for 20 minutes each, for the chromium sludge. This repetition was necessary due to the highly cohesive nature of the chromium sludge to collect a sufficient quantity of fine material for the tests.

Figure 2 – Different particle size of fillers derived from sieving method

3.2.2 Density Determination

One of the most critical specifications of the materials utilized in the production of asphalt mixtures is their density. The determination of particle density is considered an essential prerequisite for the accurate execution of volumetric mix design. Because asphalt mixtures are proportioned by volume but batched by mass during production, precise density measurements of the individual fillers and aggregates are required to properly calculate mass-to-volume conversions. Furthermore, these values are mathematically necessary to determine fundamental volumetric parameters of the compacted mixture, such as Voids in Mineral Aggregate (VMA) and the percentage of air voids. Consequently, any inaccuracies in the density characterization of the mineral phase can lead to improper binder content estimations, which would ultimately compromise the overall durability, stability, and mechanical performance of the resulting mastic and asphalt mixture.

Before determining the particle density of the specific mineral fillers, the baseline properties of the liquids used in the tests were established. First, the density of the distilled water was calculated in strict accordance with the BS EN 12697-6 standard. This reference value is directly dependent on the test temperature and was determined using the Equation 1:

$$P_w = 1{,}00025205 + \left(\frac{7{,}59\,t - 5{,}32\,t^2}{10^6}\right) \qquad \text{Eq.1}$$

where:

t represents the exact temperature of the water in °C;

P_w represents the calculated density of the water in Mg/m^3.

This calculated water density was subsequently utilized to calibrate the exact volumes of the pyknometers used in this study. The calibration was performed using the BS EN 1097-7, (2022) annex A relationship:

$V_p = \frac{m_3 - m_0}{P_w}$ Eq.2

where:

V_p stands for the volume of the pyknometer in milliliters;

m_0 is the mass of the empty pyknometer;

m_3 is the mass of the pyknometer fully filled with water.

Furthermore, because alcohol was required for testing the highly cohesive chromium sludge, the precise density of the alcohol was also determined using the calibrated pyknometers. The calculation was performed using Equation 3 from BS EN 1097-7, (2022) annex B:

$P_{alcohol} = \frac{m_4 - m_0}{V_p}$ Eq.3

where:

$P_{alcohol}$ is the density of the alcohol;

m_4 represents the mass of the pyknometer filled entirely with alcohol;

m_0 is the mass of the empty pyknometer;

V_p is the calibrated volume of the pyknometer.

As filler density is a critical parameter for accurate volumetric proportioning, the particle density of the selected fillers was determined using the pyknometer method, in accordance with the BS EN 1097-7, (2022) standard. The experimental procedure commenced only after the precise calibration of the apparatus and the testing fluids. For the reference Rheofiller, distilled water was utilized as the immersion liquid. To guarantee complete saturation, the filler-water mixture was allowed to rest undisturbed in the pyknometer for an extended duration. Because the Rheofiller exhibits a strong affinity for water, proper wetting and complete liquid penetration were easily achieved.

Furthermore, a vacuum technique was employed to successfully extract any entrapped air bubbles from the sample. However, connecting the small test pyknometers directly to the high-powered laboratory vacuum system posed a significant risk of glass fracture due to incompatible physical dimensions and excessive pressure. To safely solve this issue, the smaller test pyknometer was positioned inside a larger pyknometer, and the vacuum was subsequently applied to the outer vessel. This innovative configuration ensured that an equalized pressure was exerted on both the interior and exterior of the small pyknometer's glass walls. This approach significantly reduced the risk of breakage while successfully extracting the entrapped air from between the filler particles.

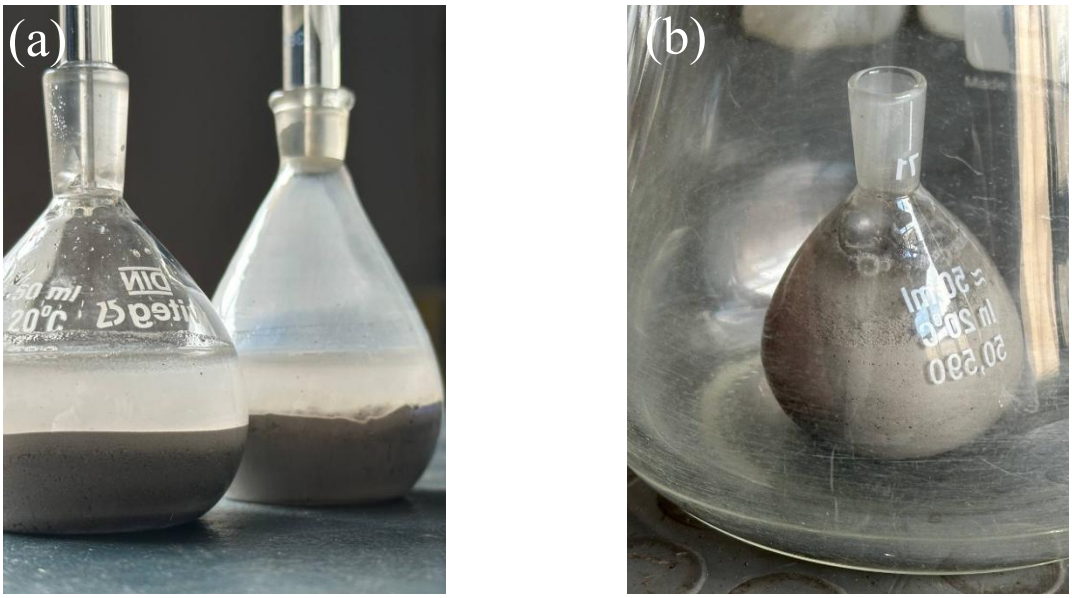

Figure 3 – Determination of Rheofiller density by use of pyknometer method a) Rheofiller submerged in Water b) De-airing Rheofiller by vacuum method inside a larger pyknometer

Conversely, methodological modifications were necessitated for the evaluation of the chromium steel sludge. As illustrated in Figure 4(a), initial trials utilizing distilled water proved unsuccessful due to inadequate water penetration, which ultimately resulted in the incomplete saturation of the sludge particles. To overcome this limitation, alcohol was employed as a substitute immersion liquid. This solvent substitution significantly enhanced the wettability of the material, thereby ensuring the accuracy of the subsequent density measurements. Consistent with the protocol established for the Rheofiller, the sludge was permitted to soak in the alcohol for a designated period to achieve full saturation. Furthermore, the identical nested-chamber vacuum configuration was implemented to safely evacuate any entrapped air residing between the solid particles.

Ultimately, the particle density of each material was derived using the Equation 4:

$$P_f = \frac{m_1 - m_0}{V_p - \frac{m_2 - m_1}{P_1}} \qquad \text{Eq.4}$$

where:

P_f represents the calculated particle density of the specific filler;

m_0 is the mass of the empty pyknometer;

m_1 is the mass of the pyknometer containing the dry filler;

m_2 is the total mass of the pyknometer containing the filler and completely filled with the liquid;

V_p is the calibrated volume of the pyknometer;

P_1 is the calculated density of the specific liquid used (water or alcohol).

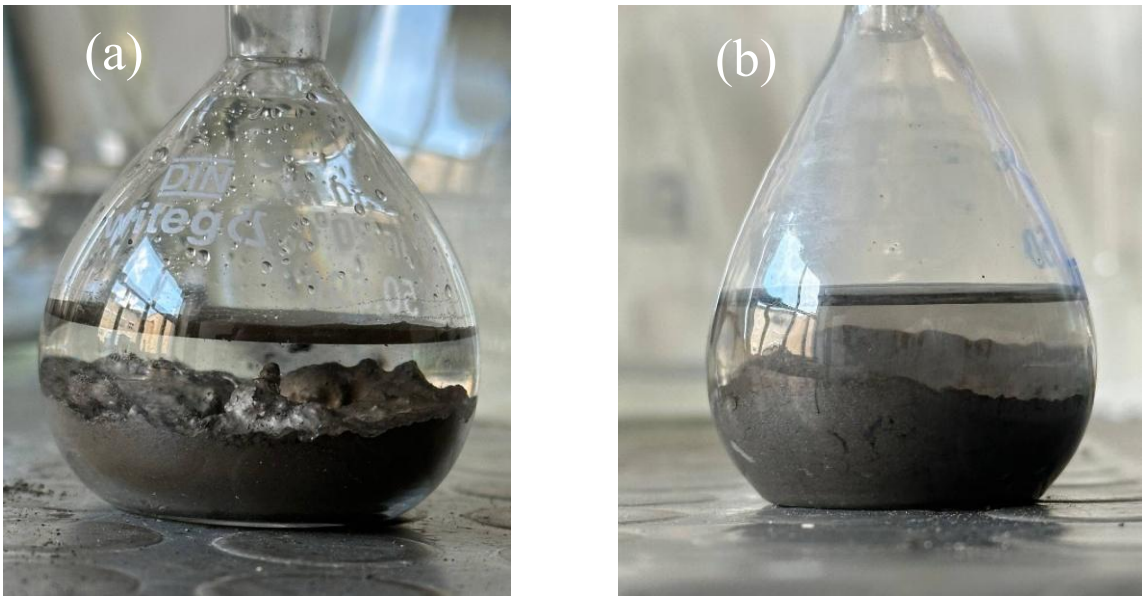

Figure 4 – Determination of Chromium Steel Sludge density by use of pyknometer method a) Chromium Submerged in Water b) Chromium Submerged in Alcohol

3.2.3 Rigden Voids Test

As recommended by EN 13043, (2002), the Rigden voids test was conducted in accordance with the BS EN 1097-4, (2008) standard to assess the void content of the dry compacted fillers. This parameter serves as a critical indicator of the filler's particle shape, surface texture, and fineness,

properties that directly influence the volume of fixed bitumen required within the mastic. In order to obtain a comprehensive overview of the packing characteristics and the inter-particle friction of the selected materials, a manual compaction methodology was strictly employed throughout the experimental phase.

To execute the procedure, a representative sample of 10 ± 1 g of the filler was carefully introduced into the test cylinder of the compaction apparatus. The material was subsequently compacted utilizing a specifically calibrated dropping weight. To ensure a consistent application of compaction energy, the weight was manually dropped 100 times at approximately one-second intervals. Following this compaction phase, the final height of the compressed filler bed was meticulously measured so that the volume of the bulk material could be accurately determined. It should be noted that while the BS EN 1097-4, (2008) standard mandates a minimum of three testing repetitions to evaluate the average void content, the experimental protocol was intentionally expanded in this study. To ensure superior statistical accuracy and to thoroughly mitigate any potential variances inherent in the manual compaction process, four independent repetitions were successfully conducted for each filler type. The final percentage of air voids was then calculated using the standard volumetric equation:

$$V_r = \left(1 - \frac{4.10^3.m_5}{\pi.\alpha^2.p_f.h}\right).100 \qquad \text{Eq.5}$$

where:

V_r is the void content expressed as a percentage;

m_5 is the mass of the compacted filler in grams;

a is the inner diameter of the dropping block cylinder in millimeters (25 mm);

p_f is the particle density of the filler in megagrams per cubic meter;

h is the measured height of the compressed filler in millimeters.

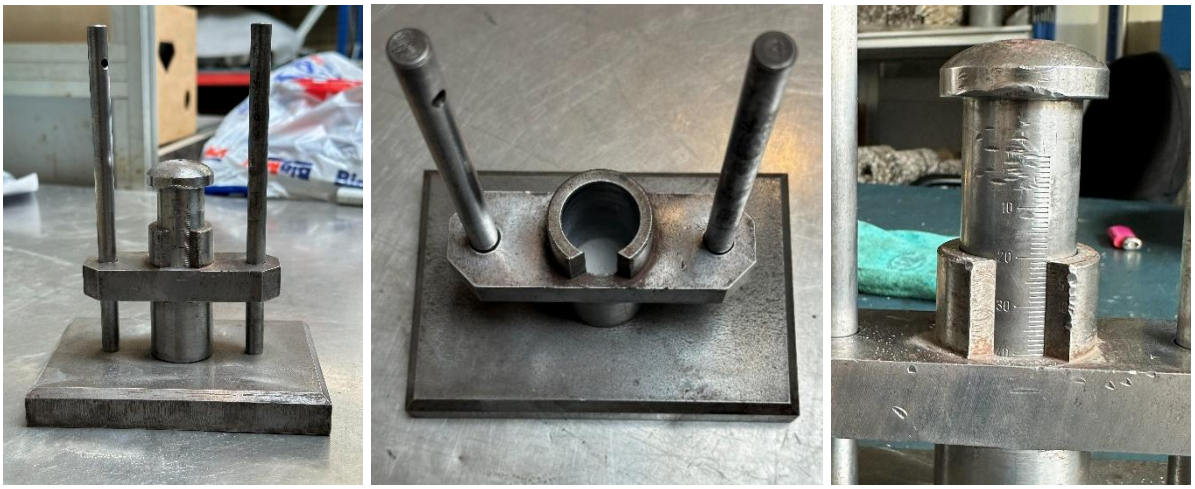

Figure 5 – Rigden void test apparatus

3.3 Mastic Preparation

3.3.1 Filler Dosage in Mastic

To obtain a comprehensive understanding of the mechanisms by which overall mastic behavior is influenced by the mineral phase, both the type of filler and its volumetric dosage were systematically investigated in this study. To achieve this objective, three distinct filler-to-bitumen (F/B) ratios were adopted throughout the experimental testing phase. A baseline F/B ratio of 1.0:1.0 was selected, as this proportion represents a conventionally used dosage within the asphalt paving industry. Alongside this baseline, two additional extreme ratios - 0.6:1.0 and 1.4:1.0 - were incorporated to represent the lower and upper practical boundaries of filler concentration, respectively. It is acknowledged that a maximum upper limit of 1.2:1.0 is formally prescribed by the Asphalt Institute, (2014). However, the highly elevated ratio of 1.4:1.0 was deliberately selected for this research. This extreme upper bound was chosen so that the critical performance thresholds and the severe stiffening behavior of the mastics could be rigorously evaluated.

Because significant variations in particle density naturally exist among the inherent filler materials, most notably the heavy chromium steel sludge, relying solely on standard weight ratios would result in vastly different volumes of solid particles within the mixtures. Therefore, instead of adopting a traditional weight-based approach, a volumetric mix design was considered.

To properly implement this, the standard commercial filler (Rheofiller) was established as the benchmark material. Its initial mass-based F/B ratios (0.6, 1.0, and 1.4) were mathematically converted into their corresponding true volumetric ratios. These newly calculated volumetric ratios were then strictly applied to calculate the required mass for the cement and chromium mastics. This volumetric approach ensures that an equivalent physical volume of solid particles is dispersed within all the evaluated mastics, thereby allowing for a fair, direct, and consistent comparison of their rheological behaviors.

To ensure clear identification and consistent referencing throughout the experimental analysis, a systematic nomenclature was adopted for all formulated mastics. Each sample was assigned a unique alphanumeric designation consisting of a literal prefix denoting the filler type, followed by a numerical suffix indicating its relative dosage. The prefixes "Rh", "Ce", and "Ch" were utilized to represent mastics containing Rheofiller, Cement, and Chromium steel sludge, respectively. For the reference Rheofiller mixtures, the numerical suffixes directly correspond to their actual mass-based filler-to-bitumen ratios (i.e., Rh 0.6, Rh 1.0, and Rh 1.4). Conversely, for the cement and chromium mastics, these same numerical designations (0.6, 1.0, and 1.4) do not represent their actual mass ratios; rather, they denote strict volumetric equivalence. For example, the designation "Ce 0.6" refers to a cement mastic formulated with a true volumetric filler concentration perfectly equivalent to that of the mass-based "Rh 0.6" reference mastic. The identical logic was applied to the chromium samples (Ch 0.6, Ch 1.0, and Ch 1.4).

Table 4 – Filler to bitumen ratio (volume ratio vs. weight ratio)

Filler type in the mastic	f/b	f/b by volume	f/b by weight	Mastic ID
Rheofiller	0.6	0.22	0.6	Rh 0.6
	1.0	0.37	1.0	Rh 1.0
	1.4	0.52	1.4	Rh 1.4
Cement	0.6	0.22	0.69	Ce 0.6
	1.0	0.37	1.15	Ce 1.0
	1.4	0.52	1.61	Ce 1.4
Chromium	0.6	0.22	1.31	Ch 0.6
	1.0	0.37	2.19	Ch 1.0
	1.4	0.52	3.06	Ch 1.4

3.3.2 Mixing Procedure

To ensure optimal workability and efficient blending, the base bitumen, the selected mineral fillers, and all associated mixing receptacles were thoroughly preheated prior to the compounding phase. The preparation of the asphalt mastics was subsequently executed utilizing a mechanical mixer equipped with a specialized two-blade impeller. Throughout the entirety of the mixing process, a controlled heating plate, positioned directly beneath the mixing container, was actively employed. This continuous thermal regulation ensured that the bituminous binder remained sufficiently fluid, a critical prerequisite for achieving structural consistency.

To prevent the agglomeration of dry particles and to promote optimal dispersion, the preheated mineral fillers were introduced into the fluid bitumen in a slow, gradual, and highly controlled manner. Furthermore, rather than restricting the mechanical agitation to a stationary or strictly horizontal plane, the mixing impeller was systematically circulated in various multi-axial directions throughout the binder matrix. This dynamic, multi-directional shearing action was deliberately applied to thoroughly disrupt any localized particle clusters and maximize the interactive surface area between the binder and the filler. Consequently, this comprehensive mixing protocol ultimately guaranteed the production of a highly uniform and exceptionally homogeneous asphalt mastic.

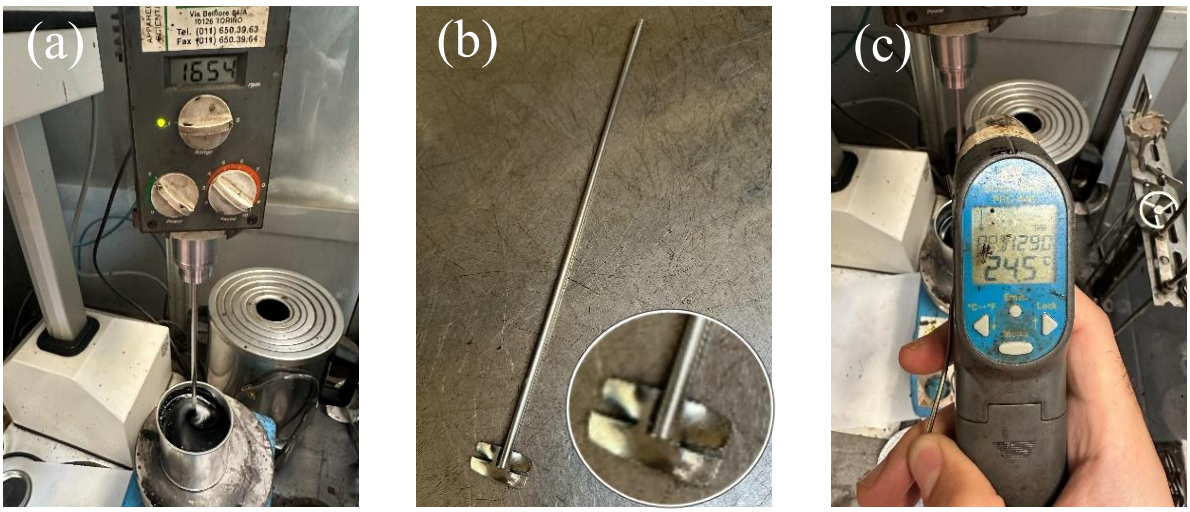

Figure 6 – Tools for preparation of mastic a) Mechanical shear mixer b) Two-Blade impeller c) Thermometer

Owing to the high density of chromium steel sludge, a greater filler mass was required to achieve the target volumetric ratio, resulting in a significant increase in mastic viscosity. Consequently, the

high-ratio chromium mastics required longer mixing durations, up to 20 minutes, and careful temperature control at high levels compared to the other mastic formulations.

Table 5 – Mixing conditions for mastic preparation

f/b ratio	Filler type	Mixing duration (minutes)	Rotation speed (rpm)	Temperature (°C)
0.6	Rheofiller	5	1240	125
	Cement	5	1250	125
	Chromium	5	1240	125
1	Rheofiller	8	1290	130
	Cement	8	1300	130
	Chromium	15	1385	140
1.4	Rheofiller	10	1450	135
	Cement	10	1550	135
	Chromium	20	1650	150

3.4 Aging Simulation

In order to study the effect of filler type and filler content on the aging of the bituminous binder, a single aging process was adopted. Thus, in addition to the virgin mastics, a corresponding set of aged mastics and virgin bitumen was prepared to simulate the long-term aging that occurs during the service life of a pavement. This aging process was carried out using a Pressure Aging Vessel (BS EN 14769, 2023). Before being placed into the conditioning vessel, all mastics and the virgin bitumen were heated in an oven at 130 °C for one hour to ensure adequate fluidity. To achieve a uniform material layer thickness of 3.2 mm inside the sample plates, the precise mass required for each specific mastic was calculated based on its previously measured density, and the material was subsequently poured.

Although standard protocols, such as BS EN 14769, (2023), require performing a short-term aging step (like using a Rolling Thin Film Oven Test (RTFOT)) prior to long-term aging, this initial step was intentionally omitted in this study. This methodological decision is supported by recent literature, which highlights that the elevated stiffness of unaged mastics significantly limits their

flowability during the RTFOT procedure (Carvajal-Muñoz & Airey, 2025; Lesueur et al., 2016; H. Li et al., 2019).

The aging conditions were controlled throughout the procedure. The samples were subjected to a constant temperature of 110 °C and an air pressure of 2.1 MPa for a continuous duration of 20 hours. Furthermore, based on a progressed mastic aging method proposed by Xing et al., (2020) baking paper was utilized to line the bottom of the sample pans. This simple modification was implemented to ensure the complete and easy recovery of the mastic samples after the high-pressure aging process was finished, thereby successfully maintaining the precise volumetric ratio for the subsequent rheological tests.

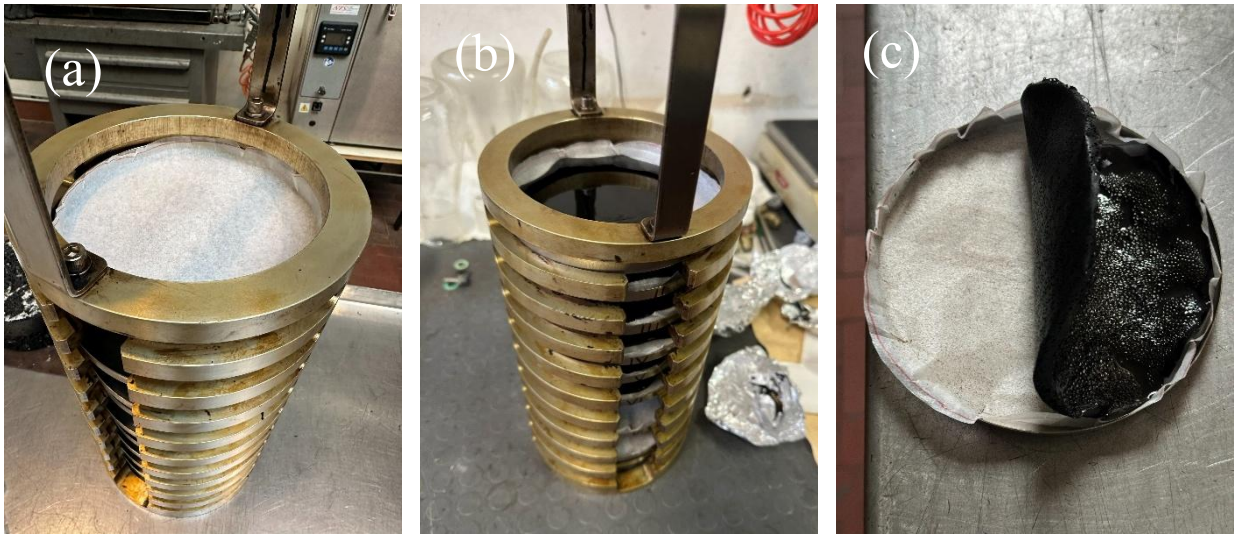

Figure 7 – Aging simulation of the mastics by use of PAV a) Use of baking paper in PAV containers b) Set of containers in the tray holder of PAV machine c) Removal of aged mastic

3.5 Frequency Sweep Test and Master Curve Construction

To evaluate the linear viscoelastic properties of the mastics, frequency sweep tests were performed using a Dynamic Shear Rheometer (DSR). To ensure accurate measurements across the entire temperature range and to comply with the equipment's torque limitations, two distinct parallel plate geometries were utilized. For the lower temperature range of 4 °C to 34 °C, an 8 mm diameter plate with a 2 mm gap was selected. Conversely, for elevated temperatures ranging from 34 °C to 82 °C, a larger 25 mm diameter plate with a 1 mm gap was employed (Airey, 2003; BS EN 14770, 2012; Yeganeh et al., 2020).

Following the laboratory tests, the linear viscoelastic behavior of the material was analyzed by developing master curves of the complex shear modulus. This was achieved by applying the Christensen-Anderson rheological model combined with the time-temperature superposition principle. The Christensen & Anderson, (1992) model is particularly well-suited for describing the viscoelastic transition behavior of bituminous materials. In this mathematical model, the complex shear modulus is calculated using the Equation 6:

$$G^*(\omega_r) = G_g \left[1+\left(\frac{\omega_0}{\omega_r}\right)^{\frac{\log 2}{R}}\right]^{-\frac{R}{\log 2}} \qquad \text{Eq.6}$$

where:

$G^*(\omega_r)$ represents the complex shear modulus at the reduced angular frequency;

G_g stands for the glassy shear modulus of the material;

ω_r is the reduced angular frequency;

ω_0 represents the crossover frequency;

R is the rheological index, which is a critical parameter because it controls the breadth of the relaxation spectrum and defines the overall shape of the viscoelastic transition region.

To construct a continuous master curve, the experimental data collected at various temperatures must be horizontally shifted. The reduced angular frequency ω_r used in the previous model was obtained by shifting the experimental data according to the Equation 7:

$$\omega_r = \omega\, a_T \qquad \text{Eq.7}$$

where:

ω_r is the reduced angular frequency;

ω is the actual angular frequency at the test temperature;

a_T is the time-temperature shift factor.

These required shift factors were calculated using the Williams-Landel-Ferry (WLF) equation, with a standard reference temperature strictly set at 20 °C. The applied formula is:

$$\log(a_T) = -\frac{C_1(T-T_{\text{ref}})}{C_2+(T-T_{\text{ref}})} \quad \text{Eq.8}$$

where:

T represents the specific test temperature in °C;

T_{ref} represents the standard reference temperature (equal to 20 °C in this study);

C_1 and C_2 are empirically determined constants.

These parameters are used to accurately determine how the material's internal relaxation time changes in response to the testing temperature, allowing the individual frequency sweeps to be smoothly combined into a single master curve.

3.6 Healing Test Methodology

3.6.1 Amplitude Sweep Test

Before initiating the healing protocol, preliminary Amplitude Sweep tests were conducted on all evaluated mastic configurations to define the appropriate damage conditions. The primary objective of these preliminary tests was to identify a specific strain level and temperature that would successfully induce measurable micro-damage without causing a catastrophic failure of the specimen. The selection of these testing parameters is based on a critical structural trade-off. If the applied strain is too low in a considered temperature, the material remains safely within its Linear Viscoelastic region. Under these conditions, no internal damage occurs, which makes it impossible to subsequently measure any healing behavior. Conversely, if the applied strain is too high in the considered temperature, the internal structure of the specimen is completely destroyed, leading to macroscopic failure and rendering any structural recovery impossible. Therefore, these preliminary tests were essential to precisely pinpoint the exact strain amplitude required to initiate repairable fatigue damage before starting the main Time Sweep protocols.

3.6.2 Specimen Conditioning and Reference Modulus Determination

The healing behavior of the asphalt mastics was evaluated using a time sweep-based protocol conducted with a DSR. Three unaged mastics containing different filler-to-binder ratios were tested. To ensure consistency, all evaluations were performed under strain-controlled conditions using an 8 mm diameter parallel plate geometry configured with a 2 mm gap.

Prior to the initiation of the actual healing tests, each specimen was carefully conditioned inside the rheometer at a constant temperature of 20 °C for a duration of 30 minutes. Throughout this conditioning period, a very low oscillatory shear strain of 0.01% was applied. This minimal strain allowed the evolution of the complex shear modulus to be continuously monitored without inducing any premature mechanical damage to the sample. Following the completion of this initial phase, a larger shear strain amplitude of 2% was applied to the specimen in a time sweep mode, and the corresponding complex shear modulus was precisely recorded. This specific measurement was established as the baseline reference modulus for all subsequent fatigue phases, allowing the exact point of required structural reduction to be calculated.

3.6.3 Fatigue Damage Criterion

For both of the evaluated healing protocols, the fatigue loading phase was strictly terminated when the complex shear modulus experienced a 35% decrease relative to its undamaged reference value. This specific 35% damage threshold was selected as a consistent and reliable criterion to safely stop the loading and initiate the subsequent rest and healing phase (AASHTO - T 391-20, 2021; Santagata et al., 2022). Applying this uniform damage level ensured that all samples experienced the same relative degree of internal micro-cracking, allowing for a fair and direct comparison of the healing capabilities across all the tested mastics.

3.6.4 Healing Test Protocols

To evaluate the healing behavior and isolate actual micro-damage healing from time-dependent phenomena, such as steric hardening, two complementary testing protocols were adopted. These procedures were designed based on the methodology proposed by Santagata et al., (2022), in their study regarding the effect of temperature on the self-healing properties of bituminous binders. These two specific procedures are known as the Fatigue-Rest-Fatigue (FRF) protocol and the Rest-Fatigue (RF) protocol.

Prior to the execution of the primary healing protocols, a systematic trial-and-error procedure, guided by the viscoelastic boundaries of the previously constructed master curves, was conducted to establish the optimal testing temperature and applied strain amplitude. The primary objective of this preliminary phase was to identify a specific temperature-strain configuration that would consistently induce fatigue failure - defined in this study as a 35% reduction in the initial complex

modulus - within a practical and logically bounded timeframe for all evaluated mastic types. For instance, initial trials demonstrated that applying an excessively low strain coupled with a higher testing temperature resulted in an impractically prolonged loading period before the targeted failure could be achieved. Conversely, excessive strain led to premature, abrupt failure, precluding any meaningful observation of progressive damage. Furthermore, it was critically important to select an exceptionally low strain amplitude for use during the initial conditioning and subsequent rest periods. This precaution was strictly enforced to ensure that the continuous measurement of the complex modulus did not inadvertently inflict structural micro-damage onto the specimens, particularly given the broad variations in inherent stiffness among the different formulated mastics.

3.6.4.1 FRF Protocol

In the FRF protocol, as illustrated in Figure 8, the specimen was initially subjected to cyclic shear loading at 20 °C using a strain amplitude of 2% in a time sweep mode. This part is highlighted in dark gray on the left side of the diagram. This loading phase was continued until a 35% reduction in the complex shear modulus was reached, which marked the end of the first fatigue stage. For simulating the healing phenomena, both time and temperature effect is considered. Thus, immediately after the first fatigue stage, a rest period with a total duration of two hours was applied to allow for healing. This rest phase consisted of two specific temperature stages: 90 minutes at 30 °C followed by 30 minutes at 20 °C. Throughout the entire rest period, a minimal oscillatory strain of 0.01% was maintained to safely monitor the recovery of the complex shear modulus without introducing any additional mechanical damage. The rest period is highlighted in light gray in the center of the Figure 8. Once the rest phase was completed and the temperature was stabilized back at 20 °C, a second fatigue phase was initiated using the original 2% strain amplitude. The loading was continued until the modulus experienced the 35% reduction for the second time, calculated relative to the recovered modulus value recorded at the exact beginning of this second fatigue phase.

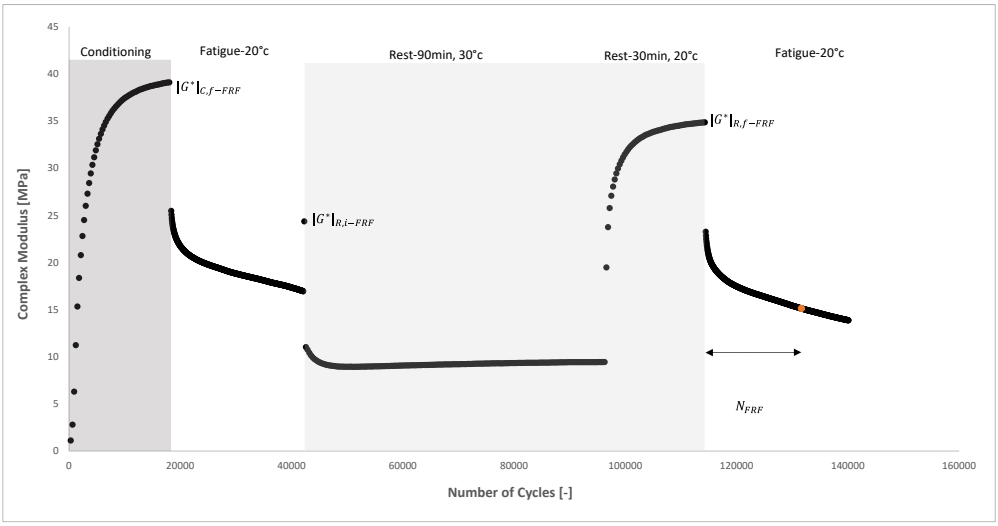

Figure 8 – Schematic of FRF testing protocol

3.6.4.2 RF Protocol

The RF protocol was conducted in parallel with the FRF tests to carefully isolate the effects of time-dependent material evolution from actual damage-induced healing. In this specific protocol, after the initial conditioning step (illustrated in Figure 9, highlighted in dark grey on the left part of the diagram), the undamaged specimen was subjected to a rest period identical to the one used in the FRF test (90 minutes at 30 °C followed by 30 minutes at 20 °C). During this rest phase, a very low oscillatory strain was applied to prevent any fatigue damage initiation, which allowed the material to undergo only time-dependent structural changes. Following this rest phase, a single sinusoidal fatigue loading stage was executed at 20 °C using the exact same strain amplitude and frequency. By keeping all test parameters entirely identical - including the temperature, frequency, strain level, and rest duration - the RF results provided a reliable reference response. This reference enabled the clear separation of true micro-damage healing from the stiffness variations caused purely by steric hardening during the rest period.

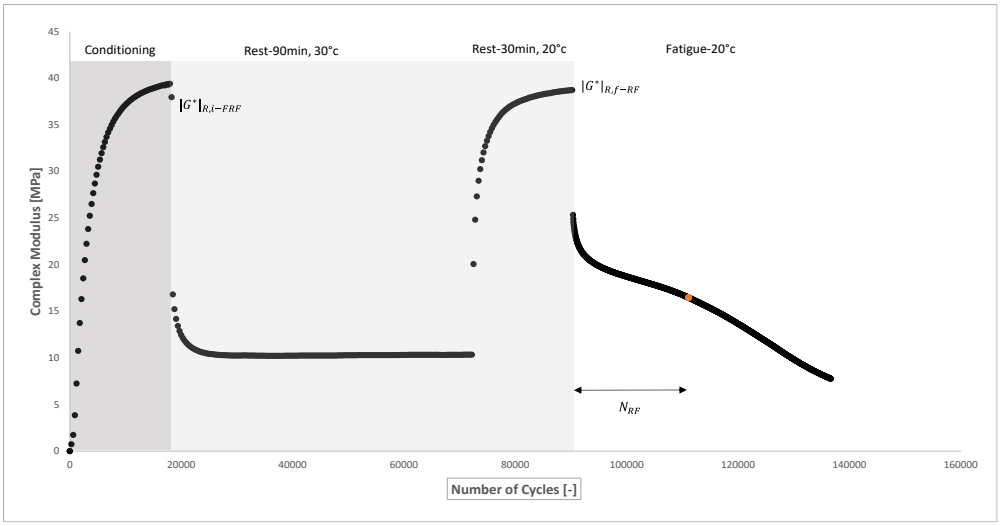

Figure 9 – Schematic of RF testing protocol

3.6.5 Self-Healing Index (I_G)

To quantitatively evaluate the self-healing ability of the mastics, a specific stiffness recovery index, denoted as I_G, was defined. This index accounts for the stiffness loss that occurs during the initial fatigue phase and mathematically subtracts the contribution of the time-dependent effects measured during the Rest-Fatigue test (Miglietta et al., 2021). The index is calculated using the following formula:

$$I_G = \frac{\Delta|G^*|_{R-\mathrm{FRF}} - \Delta|G^*|_{R-\mathrm{RF}}}{\Delta|G^*|_{F-\mathrm{FRF}}} . 100 \qquad \text{Eq.9}$$

where:

$\Delta \mid G^* \mid_{R-\mathrm{FRF}}$ represents the difference between the complex modulus recorded at the end of the rest period and the modulus recorded at the end of the first fatigue phase in the FRF test;

$\Delta \mid G^* \mid_{R-\mathrm{RF}}$ is the corresponding modulus difference measured in the RF test, which represents the recovery driven strictly by time-dependent phenomena rather than damage repair;

$\Delta \mid G^* \mid_{F-\mathrm{FRF}}$ is the total modulus loss measured during the first fatigue phase of the FRF test.

By subtracting the reference contribution, a precise measure of the true stiffness recovery achieved through micro-damage healing is provided. In this study, this index was applied to all tested mastics, allowing a direct and accurate comparison of their self-healing performance.

3.6.6 Fatigue Endurance Index (I_N)

A second performance indicator, denoted as the fatigue endurance index or I_N, was introduced to quantify the relative extension of the material's fatigue life after the rest period. This specific index evaluates how many additional loading cycles a specimen can withstand after experiencing initial fatigue damage and subsequent recovery, compared to its original fatigue resistance under completely undamaged conditions (Miglietta et al., 2021). The index is mathematically defined by the Equation 10:

$$I_N = \frac{N_{\mathrm{FRF}}}{N_{\mathrm{RF}}}.100 \qquad \text{Eq.10}$$

where:

N_{FRF} represents the exact number of loading cycles sustained during the second fatigue phase of the FRF test, which is the number of cycles required for the complex shear modulus to reach a 35% reduction after the healing period is completed;

N_{RF} represents the number of loading cycles required to reach that exact same 35% reduction threshold under undamaged conditions, as measured during the RF test.

This formulation effectively normalizes the fatigue endurance of a previously damaged and healed specimen against its intrinsic fatigue resistance. Consequently, a higher value of I_N indicates that the material is able to successfully withstand a greater number of loading cycles after healing, which reflects a much more effective self-healing capability. In this study, this index was utilized to directly compare the fatigue-healing performance of mastics containing different filler-to-binder ratios, allowing the clear identification of the specific mixtures that exhibit structural recovery behavior.

Chapter 4: Results and Discussions

4.1 Initial Characterization

Following the methodology outlined previously, the baseline properties of the immersion liquids and the exact volumes of the test pyknometers were experimentally determined. During the initial laboratory procedure, the test temperature of the distilled water was precisely measured at 25.2 °C. Applying this recorded temperature to the standard polynomial equation yielded a calculated water density of 0.9971 Mg/m^3.

Using this established reference water density, the precise volumes of the two pyknometers were calibrated. Table 6 presents the measured volumes of the pyknometers.

Table 6 – Pyknometers calibration

Pyknometer ID	mass of empty pyknometer (g)	mass of pyknometer filled with water (g)	pyknometer volume (Mg/m^3)
1	33.268	83.486	50.37
2	26.813	78.191	51.53

Finally, utilizing these newly calibrated pyknometers, the precise density of the alcohol which was strictly required to properly evaluate the highly cohesive chromium sludge was determined. Across the test replicates, the average density of the alcohol was calculated equal to 0.802 Mg/m^3.

Table 7 – Calculation of alcohol density

Pyknometer ID	mass of empty pyknometer (g)	mass of pyknometer filled with alcohol (g)	pyknometer volume (cm^3)	alcohol density (Mg/m^3)	Average value (Mg/m^3)
1	33.268	73.256	50.37	0.794	0.802
2	26.813	68.601	51.53	0.811	

4.1.2 Filler Density Determination

Following the calibration of the pyknometers and liquids, experimental mass measurements were recorded to determine the exact particle densities of the Rheofiller and the chromium steel sludge. The density of the ordinary Portland cement was not experimentally measured in this phase, as its standard particle density is widely established and accepted as 3.10 Mg/m^3 in paving practices.

Applying the standard formula detailed in the methodology, the final densities for the tested materials were calculated. The reference Rheofiller exhibited a density of 2.72 Mg/m^3. In stark contrast, the chromium steel sludge yielded a significantly higher particle density of 5.91 Mg/m^3. As previously noted, this substantial difference in physical mass mathematically justified the absolute necessity of utilizing volumetric proportioning rather than weight-based ratios during the subsequent mastic preparation phase.

The exact measured masses, the specific pyknometer volumes utilized, the density of the corresponding liquids, and the final calculated particle densities (P_f) for the experimentally tested fillers are summarized in Table 8.

Table 8 – Experimental measurements and calculated particle densities of the fillers

Filler type	Liquid used	P_l (Mg/m^3)	V_p (ml)	m_0 (g)	m_1 (g)	m_2 (g)	Density P_f (Mg/m^3)	Average Density (Mg/m^3)
Rheofiller	Water	0.9971	51.53	26.811	43.197	88.567	2.7040	2.72
			50.37	33.269	52.596	95.79	2.7312	
Chromium Sludge	Alcohol	0.8021	51.53	26.813	37.317	77.221	5.9017	5.91
			50.37	33.268	44.029	82.969	5.9183	

4.1.3 Fillers Particle Size Distribution

The particle size distribution of the bulk filler materials was evaluated using a standard mechanical sieve analysis. Prior to the sieving process, the entire raw samples of Rheofiller, ordinary Portland cement, and chromium steel sludge were placed in an oven and dried overnight at a constant temperature of 110 °C to eliminate any residual moisture. To determine the complete gradation of the materials, a standard series of sieves was employed. This series consisted of 2 mm, 500 µm, 250 µm, 125 µm, 75 µm, and 63 µm meshes, terminating with a solid collection tray at the bottom.

Following the mechanical shaking, the passing percentages for each sieve size were calculated to construct the gradation curves. Particular attention was directed toward the material fraction passing the 125 µm sieve, as only this specific fine fraction was isolated and utilized for the subsequent mastic preparation. The laboratory results indicated significant variations in the initial fineness of the raw materials. As it can be seen in the Figure 10 for the ordinary Portland cement, it was observed that approximately 92% of the total mass passed through the 125 µm mesh, indicating a highly refined raw product. In contrast, the reference Rheofiller exhibited a somewhat coarser initial gradation, with roughly 62% of the material passing this target sieve. Finally, the raw chromium steel sludge was found to be the most coarse of the three evaluated materials, with only about 40% of the bulk material passing the 125 µm threshold. Because of this relatively low passing percentage, the previously mentioned repeated mechanical vibration was necessary to harvest a sufficient quantity of the fine fraction required for the volumetric mix design.

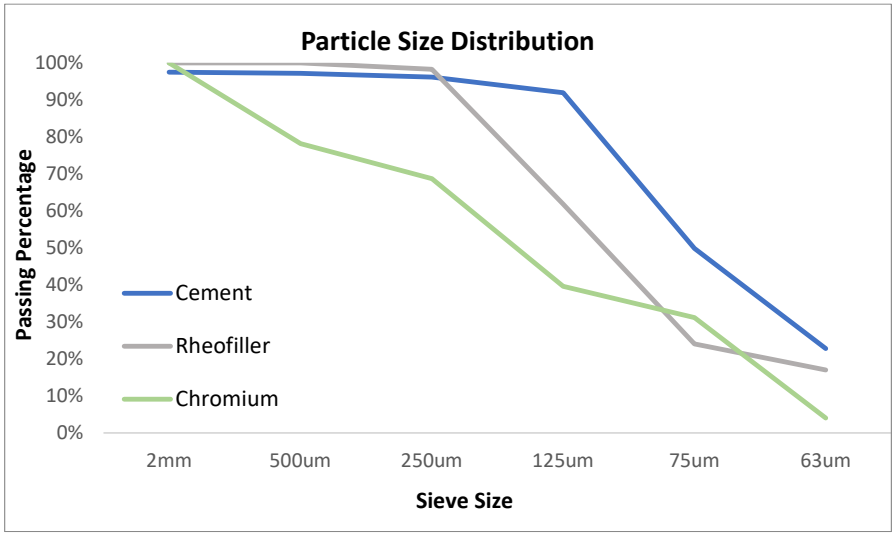

Figure 10 – Particle size distribution of three fillers

4.1.4 Fillers Rigden Voids Test Results

The Rigden voids of each filler of the study has been determined as explained in previous chapter. In order to ensure the statistical reliability of the measurements, the dry compaction procedure was performed with four independent repetitions for each of the three evaluated filler types. The experimental data demonstrated high precision, with standard deviations remaining below 0.3% across all tested materials. Following the calculations, a significant variation in the volumetric packing behavior of the fillers was revealed. The reference Rheofiller exhibited the most efficient packing, resulting in the lowest mean Rigden void content of 31.7%. The ordinary Portland cement was characterized by an intermediate mean porosity of 45.1%. In stark contrast, the chromium steel sludge yielded the highest internal porosity, with a calculated mean Rigden void content of 59.0%.

Table 9 – Experimental measurements and calculated rigden void

Filler type	Repetition Number	Compacted mass (g)	Filler density	Compressed filler height (mm)	Rigden void	Average
Rheofiller	1	9.88	2.7	10.98	32.1%	31.7%
	2	9.92		11	31.9%	
	3	9.97		11	31.6%	
	4	10.01		11.01	31.4%	
Cement	1	10.02	3.1	12	45.1%	45.1%
	2	9.99		12	45.3%	
	3	9.99		11.95	45.0%	
	4	10.02		11.99	45.1%	
Chromium steel	1	10.03	5.91	8.45	59.1%	59.0%
	2	10.01		8.4	58.9%	
	3	10.03		8.41	58.9%	
	4	9.98		8.4	59.0%	

The magnitude of the Rigden voids serves as a critical indicator of a filler's specific surface area, particle shape irregularity, and overall fineness. A higher rigden void percentage implies that the solid particles pack together less efficiently, thereby leaving a larger volume of empty space between them. Within an asphalt mastic, these interstitial voids must be completely filled by the bituminous binder before any excess bitumen can act as a lubricant. The bitumen that becomes trapped within these voids is commonly referred to as "fixed bitumen," whereas the remaining binder is known as "free bitumen" (Zheng et al., 2018). Because the chromium steel sludge

exhibited a remarkably high Rigden void content of 59.0%, it was determined that this specific industrial by-product would absorb a significantly larger proportion of the neat bitumen simply to coat its particles and fill its internal voids. Consequently, a reduced volume of free bitumen would be available to facilitate the flow of the material, which was predicted to lead to a much stiffer and more viscous mastic compared to the reference mixtures. Conversely, the relatively low Rigden void content of the Rheofiller (31.7%) indicated that a greater volume of free bitumen would remain within the matrix, thereby promoting a more workable and less rigid asphalt mastic. Sitting between these two extremes, the ordinary Portland cement was predicted to offer an intermediate stiffening effect on the final material (Faheem & Bahia, 2010).

4.2 Rheological Characterization

4.2.1 Effect of Filler Ratio

The rheological behavior of the asphalt mastics in their unaged state was systematically analyzed to evaluate the specific influence of the filler-to-binder ratio on the overall viscoelastic properties of the material. The stiffness of the mixtures was quantified using the complex shear modulus (G^*), a critical parameter that represents the combined elastic and viscous resistance to deformation. A higher value of G^* physically denotes a stiffer internal structure, which indicates enhanced physicochemical interactions between the bituminous binder and the dispersed solid filler particles.

The experimental results demonstrated that an increase in the filler-to-binder ratio consistently resulted in a systematic elevation of the complex shear modulus. As the volumetric concentration of the filler was increased, the mastics became stiffer. Notably, this pronounced stiffening trend was consistently observed across all evaluated filler types. This observation confirms that the overall stiffening effect is primarily governed by the volumetric concentration of the solid inclusions, largely independent of the specific mineralogical composition of the filler.

To visually illustrate this impact, the frequency sweep curves for each mastic configuration are presented in the Figure 11.

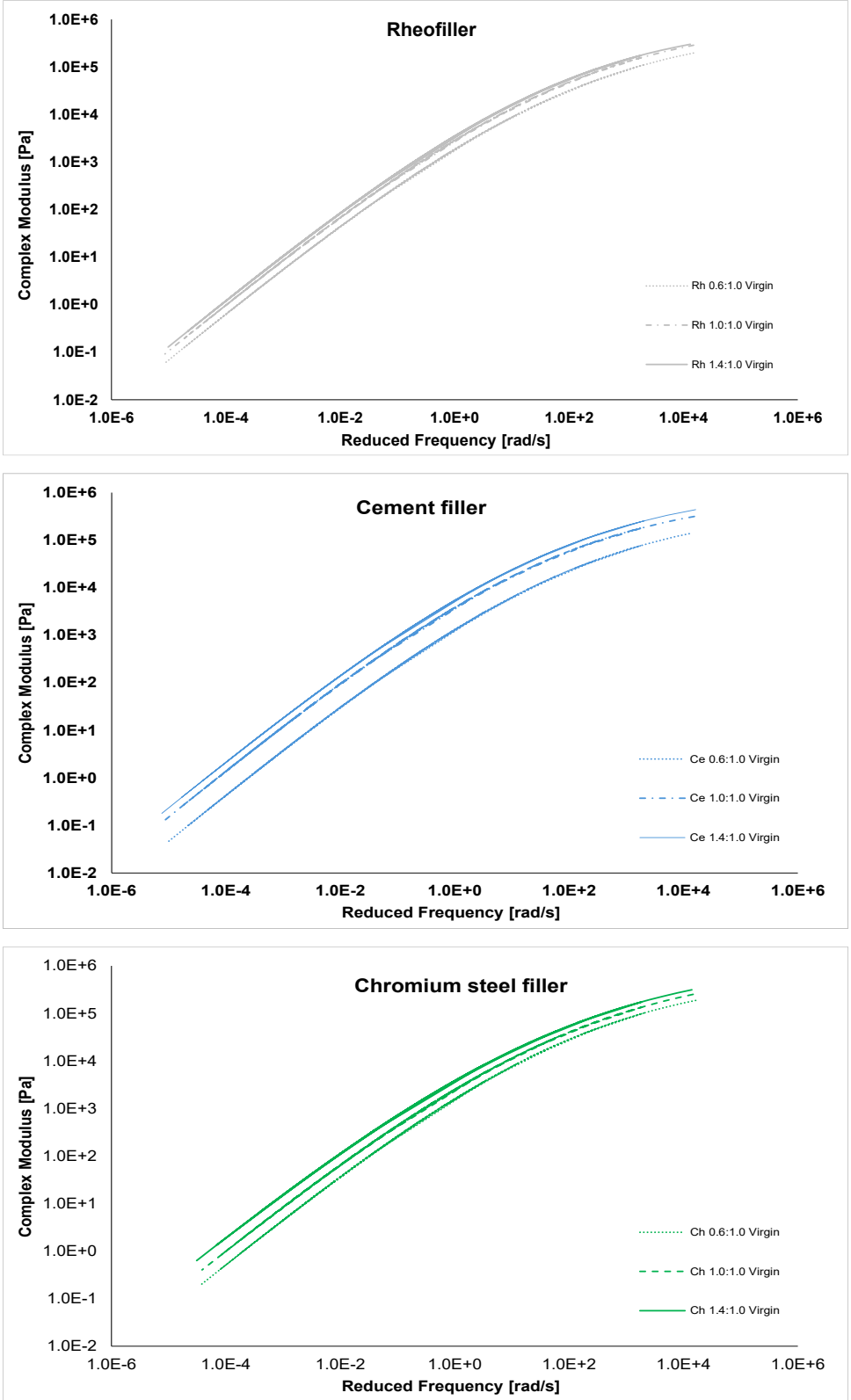

Figure 11 – Master curves of complex modulus for different mastics

Table 10 presents the master curve fitting parameters for the evaluated mastics, including the temperature shift constants (C_1 and C_2), the glassy modulus (G_g), the crossover frequency (ω_0), and the rheological index (R). All curves were constructed at a reference temperature (T_r) equal to 20 °C. The most significant indicator of material stiffening in this analysis is the crossover frequency (ω_0). As the filler-to-binder ratio increases from 0.6 to 1.4, the W_0 value consistently decreases across all filler types. For example, the ω_0 of the Rheofiller mastics drops from 89.4 at the 0.6 ratio to 63.1 at the 1.4 ratio. A lower crossover frequency physically indicates that the mastic behaves more like an elastic solid and takes longer to relax, confirming that higher volumetric concentrations of filler significantly stiffen the matrix. Furthermore, an analysis of the rheological index (R) reveals distinct behavioral trends depending on the specific filler type. For the mastics formulated with Rheofiller and cement, the R parameter remains highly stable, ranging narrowly between 1.32 and 1.37. This stability demonstrates that while the addition of these conventional fillers significantly increases the overall macroscopic stiffness, it does not fundamentally alter the natural relaxation shape of the base bitumen. Conversely, the mastics containing chromium steel sludge exhibit a wider variation and a notable increase in the rheological index, with values ranging from 1.37 to 1.56. Physically, this higher R value indicates a broader relaxation spectrum, meaning that the rheological transition from a solid-like elastic state to a fluid-like viscous state occurs much more smoothly and gradually. In direct contrast, the mastics containing traditional fillers possess a narrower spectrum and consequently undergo this phase transition at a noticeably faster and more abrupt rate. This delayed, smoother transition in the chromium samples suggests that the sludge does more than merely provide physical stiffening; its unique morphological characteristics actively create a more complex and heavily structured viscoelastic matrix compared to conventional mixtures.

Table 10 – Master curve parameters

Mastic	T_r	C_1	C_2	G_g	ω_0	R
Rh 0.6	20	16.12623	134.6812	7.03E+05	8.94E+01	1.37
Rh 1.0	20	15.95453	133.2611	9.65E+05	7.93E+01	1.35
Rh 1.4	20	16.17877	138.176	9.36E+05	6.31E+01	1.32
Ce 0.6	20	16.45447	141.2657	5.07E+05	9.61E+01	1.35
Ce 1.0	20	16.30538	135.0529	9.26E+05	5.40E+01	1.33
Ce 1.4	20	15.98512	131.519	1.35E+06	4.91E+01	1.37
Ch 0.6	20	13.32428	112.2595	6.89E+05	1.09E+02	1.37
Ch 1.0	20	13.58096	116.2151	1.06E+06	7.94E+01	1.47
Ch 1.4	20	14.48483	123.8959	1.41E+06	5.05E+01	1.56

Additionally, the G^* ratio plots reveal a pattern of diminishing returns; the relative boost in stiffness becomes smaller as the filler content increases. This behavior is consistent across all mastic types but is most obvious at high reduced frequencies which represent low temperatures.

Under these conditions, the curves on the graph begin to converge. This signals that the stiffness (G^*) becomes less sensitive to adding more filler. Essentially, at high reduced frequencies (low temperatures), the mastic stiffness hits a "plateau", a point where adding extra filler in lower temperature contributes very little to further stiffening.

Overall, these results demonstrate that while increasing the F/B ratio effectively enhances mastic stiffness, the influence of filler type remains secondary. Moreover, the diminishing variation of G^* at higher filler contents and higher frequencies highlights a saturation effect in the stiffening mechanism of asphalt mastics.

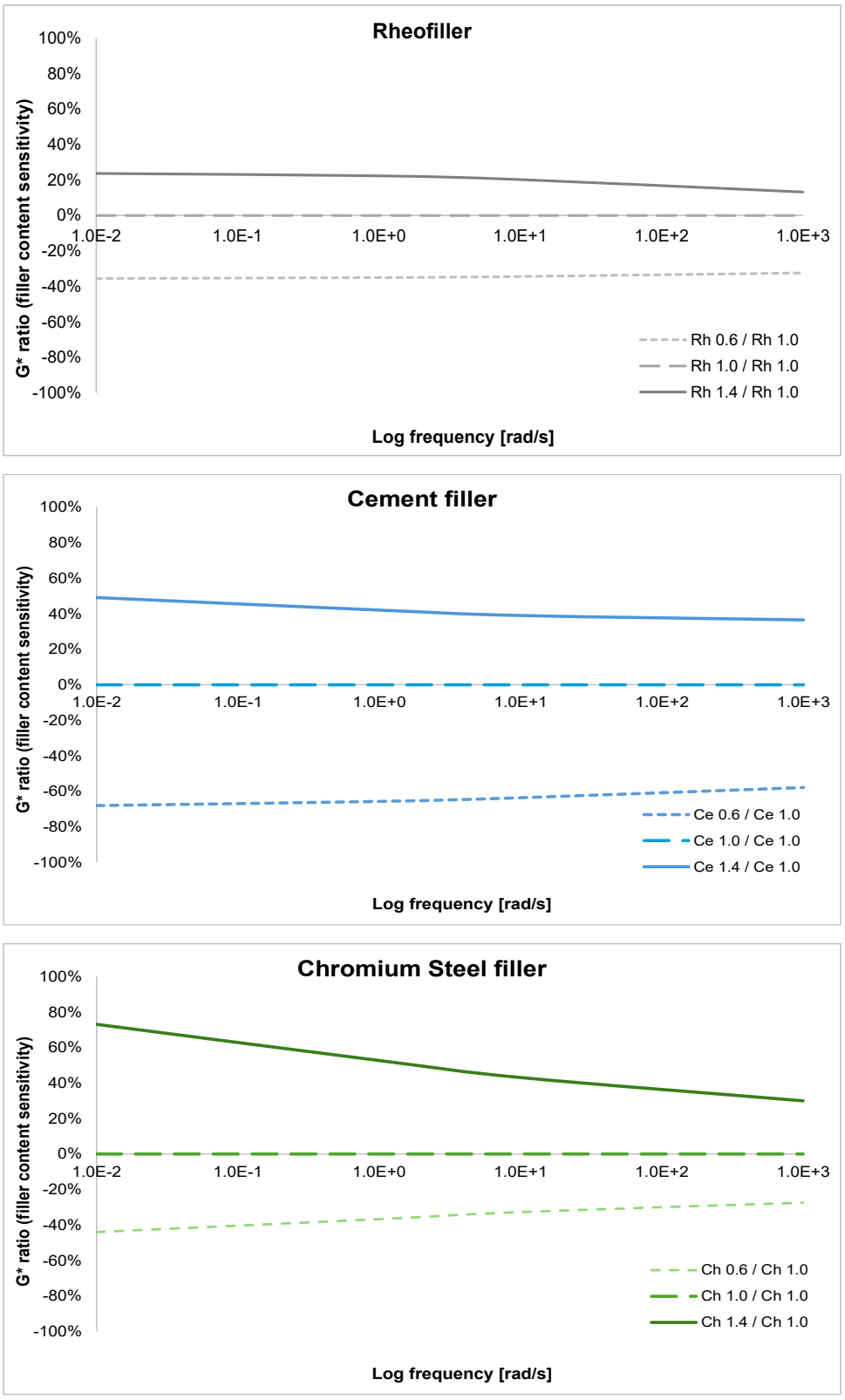

Figure 12 – Effect of filler content on mastic complex modulus

4.2.2 Effect of Filler Type

To determine how the specific type of mineral filler affects the unaged mastics, master curves of the complex shear modulus (G^*) were constructed for each filler-to-binder ratio. This analytical method allowed for a direct comparison of the material's viscoelastic behavior across a wide range of frequencies, effectively simulating various environmental temperatures and traffic loading speeds.

As it is shown in the Figure 13**,** at the lower filler-to-binder ratios of 0.6 and 1.0, the master curves exhibited very little difference between the mastics, regardless of whether they were prepared with Rheofiller, ordinary Portland cement, or chromium steel sludge. The stiffness values overlapped almost perfectly across the entire frequency range. This specific behavior indicates that when the filler content remains relatively low, the specific mineralogy of the solid particles does not play a major role. Instead, the overall rheology of the mixture is primarily dominated by the physical properties of the bitumen binder itself.

In contrast, the behavioral differences became a bit more pronounced at the highest filler-to-binder ratio of 1.4. At high reduced frequencies, which correspond to low environmental temperatures, the mastic containing the chromium sludge and Rheofiller demonstrated the lowest stiffness values. This characteristic is highly advantageous, as a material that avoids becoming overly stiff in cold conditions remains less brittle, thereby offering much better resistance to thermal cracking. Conversely, at low reduced frequencies representing high-temperature conditions, the mastics formulated with chromium and cement displayed the highest stiffness. This increased rigidity is highly beneficial for hot climates, as it helps the pavement structure effectively resist permanent deformation, such as rutting, under the pressure of heavy traffic loads.

Overall, this analysis confirmed that the fundamental influence of the filler type is highly concentration-dependent. While the mineralogical effects remained negligible at the lower volumetric ratios, the specific characteristics of the filler became a slightly more important factor in defining the mastic's high-temperature and low-temperature performance as the filler concentration was increased to its high level.

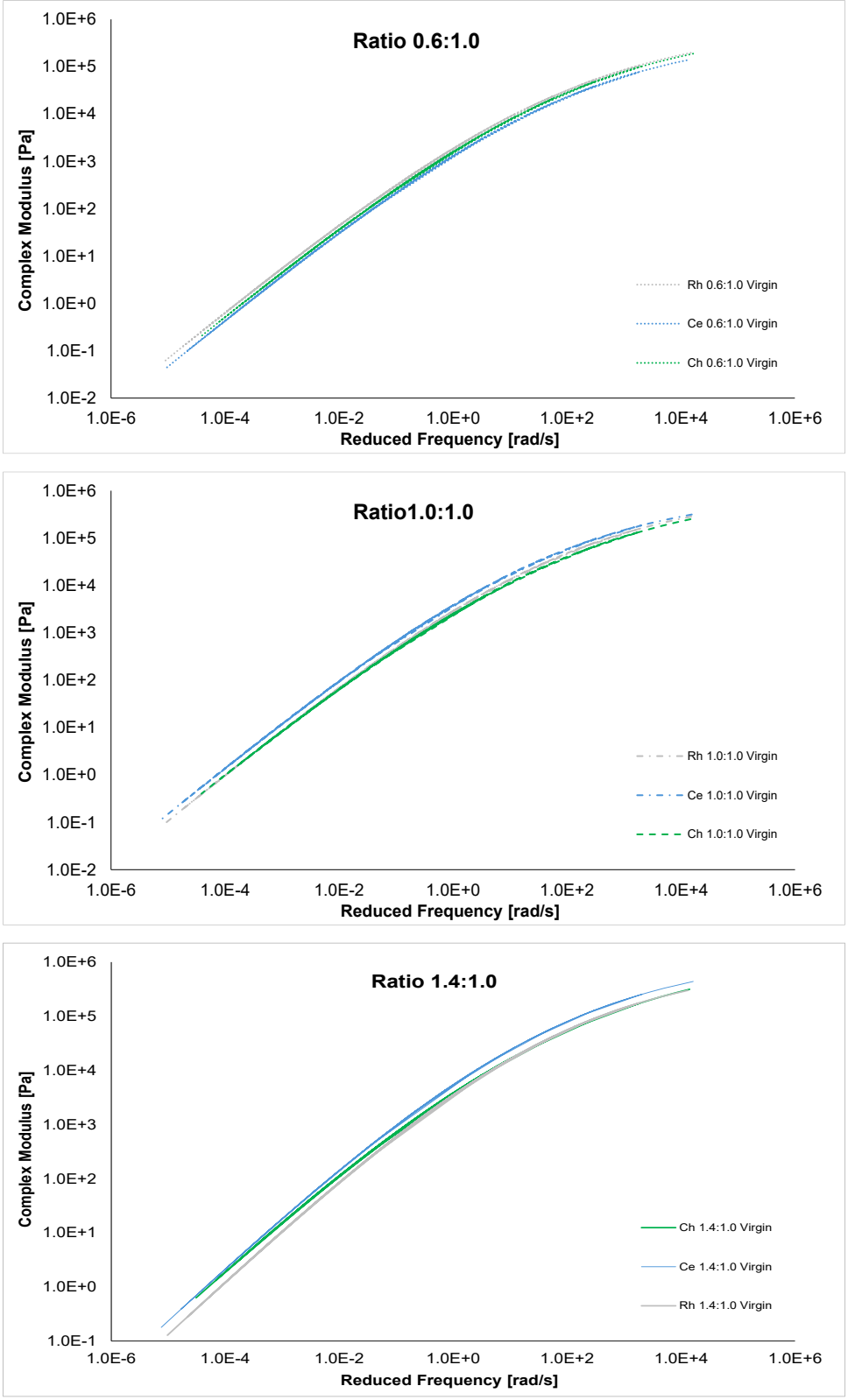

Figure 13 – Master curves of complex modulus for different filler-to-bitumen ratios

4.2.3 Effect of Filler Ratio on aging

The influence of the filler ratio on the aging susceptibility of the mastics was evaluated by calculating an aging index, which is defined as the ratio of the aged complex shear modulus to the unaged complex shear modulus (G^*_{Aged} / G^*_{Virgin}). For all evaluated mastics - incorporating Rheofiller, ordinary Portland cement, and chromium steel sludge - a clear frequency-dependent behavior was observed across the entire frequency range. The aging effect was found to be much stronger at lower frequencies. This indicates that oxidative aging primarily hardens the viscous response of the material, which fundamentally governs its performance at high temperatures. In contrast, a much smaller impact was noted on the elastic response at high frequencies, which correspond to low environmental temperatures.

When analyzing the effect of filler concentration, a consistent behavioral pattern emerged across all types of mineral fillers. As the filler-to-binder ratio was increased from 0.6 to 1.4, the Aging Index curves for the Rheofiller, cement, and chromium mastics were consistently shifted downward. The mastics formulated with the highest filler concentration (ratio of 1.4) exhibited the lowest aging susceptibility. This inverse relationship indicates that the addition of a higher volume of solid particles actively mitigates the aging-induced stiffening of the material.

These experimental observations are in strong agreement with the existing literature, specifically confirming the mechanisms proposed in the detailed study by Wu & Airey, (2011). As previously discussed, they demonstrated that the inclusion of mineral fillers generally reduces the aging susceptibility of the base binder. The results of this current study validate that as the filler content increases; the dispersed solid particles create a more comprehensive physical barrier within the bituminous matrix. This barrier effectively restricts the diffusion of oxygen into the mastic, successfully slowing down the overall oxidative reactions. Furthermore, the higher density of solid inclusions mechanically stabilizes the matrix, thereby preventing it from becoming as brittle after long-term aging as mixtures formulated with lower filler concentrations.

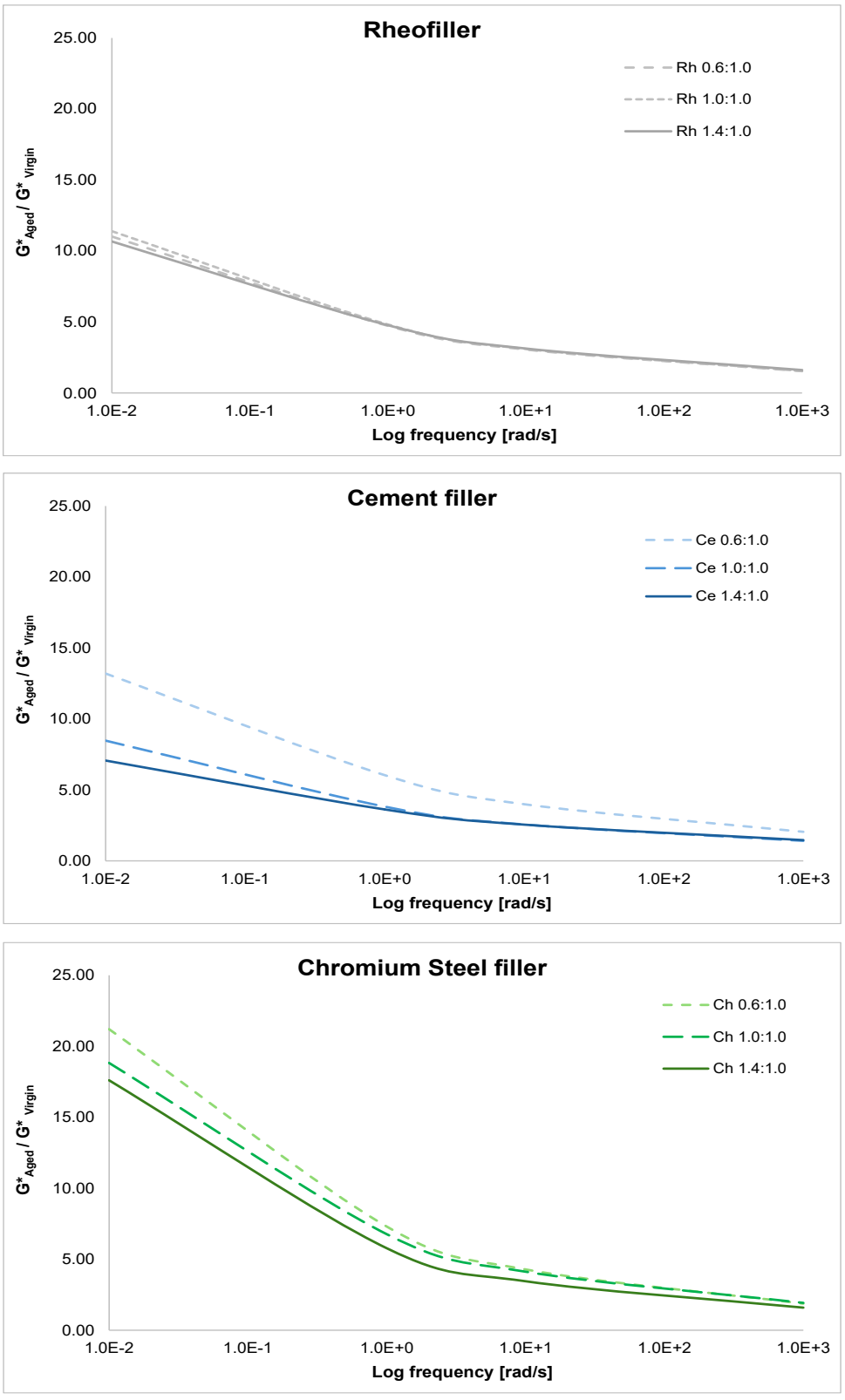

Figure 14 – Aging index of different mastics

4.2.4 Effect of aging on neat bitumen

To establish a reliable reference baseline for evaluating the aging behavior of the mastics, the long-term aging process was initially conducted on the neat bitumen. The linear viscoelastic response of the unmodified binder, both before and after aging, is illustrated in the master curves presented in Figure 15. As clearly seen in the curves, and also expected, the aging process significantly increased the complex shear modulus of the neat bitumen across the entire frequency spectrum, indicating a pronounced stiffening effect caused by oxidation.

To precisely quantify this stiffening, the aging index of the neat bitumen was calculated and is plotted in Figure 16. This specific curve serves as the critical reference line for evaluating the aging susceptibility of all three prepared mastics in the subsequent sections. As illustrated in this figure, the complex shear modulus of the unmodified binder was increased by a factor of approximately 30 at the lowest testing frequency (0.01 rad/s) following the long-term aging procedure. Conversely, at high frequencies, the aging index of the virgin bitumen was observed to drop to a value of approximately 5. This highly frequency-dependent behavior confirms that oxidative aging predominantly hardens the viscous response of the base material

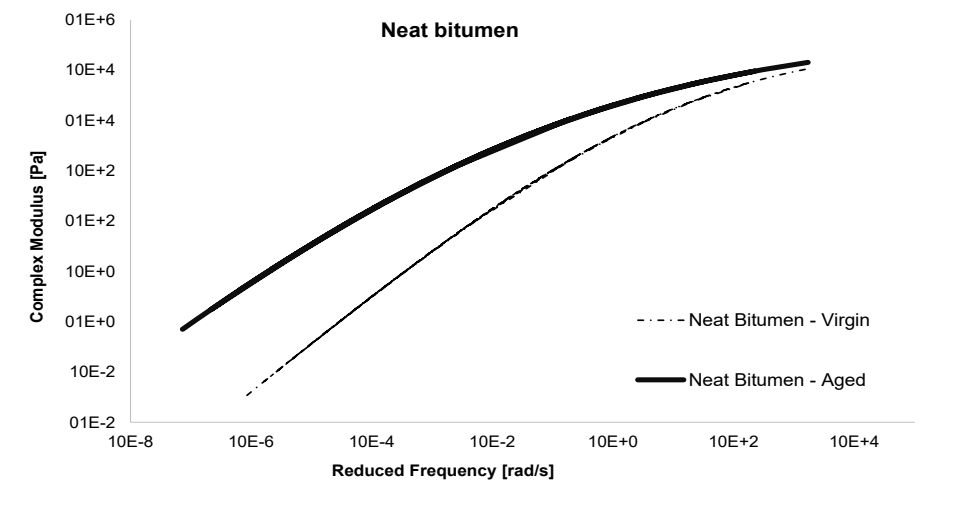

Figure 15 – Master curve of neat bitumen

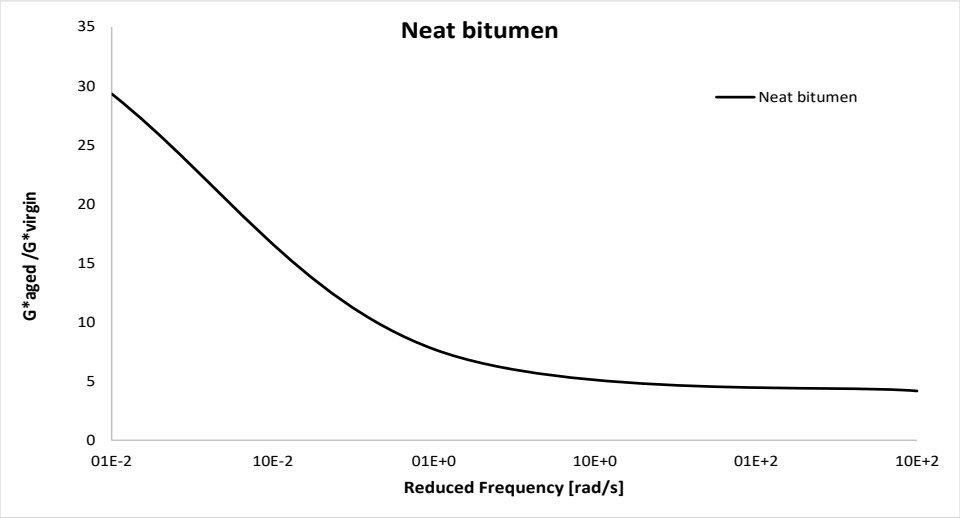

Figure 16 – Aging index of neat bitumen

4.2.5 Effect of Filler Type on aging

To isolate the effect of mineralogy and physical properties on aging susceptibility, the aging indices of the Rheofiller, cement, and chromium mastics were directly compared against the neat bitumen across three filler-to-binder ratios (0.6, 1.0, and 1.4). As illustrated in the comparative aging curves, a fundamental observation can be made: all the evaluated mastics, regardless of the filler type or volumetric ratio, exhibited significantly lower aging indices compared to the virgin bitumen reference line. This confirms that the inclusion of solid particles provides a protective physical barrier that successfully mitigates the severe oxidative hardening of the base binder.

However, when comparing the specific filler types against each other, a distinct performance hierarchy was observed. Across all evaluated filler-to-binder ratios, the mastic formulated with chromium steel sludge consistently exhibited the highest aging index among the mixtures. This indicates that while the chromium sludge does reduce the aging susceptibility compared to the neat bitumen, it is noticeably less effective at hindering the oxidative process than traditional fillers like Rheofiller and ordinary Portland cement.

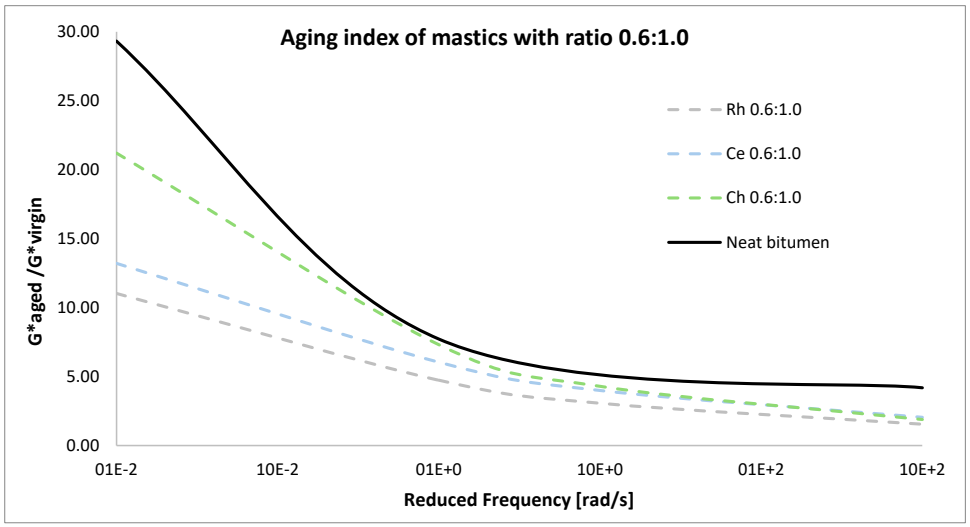

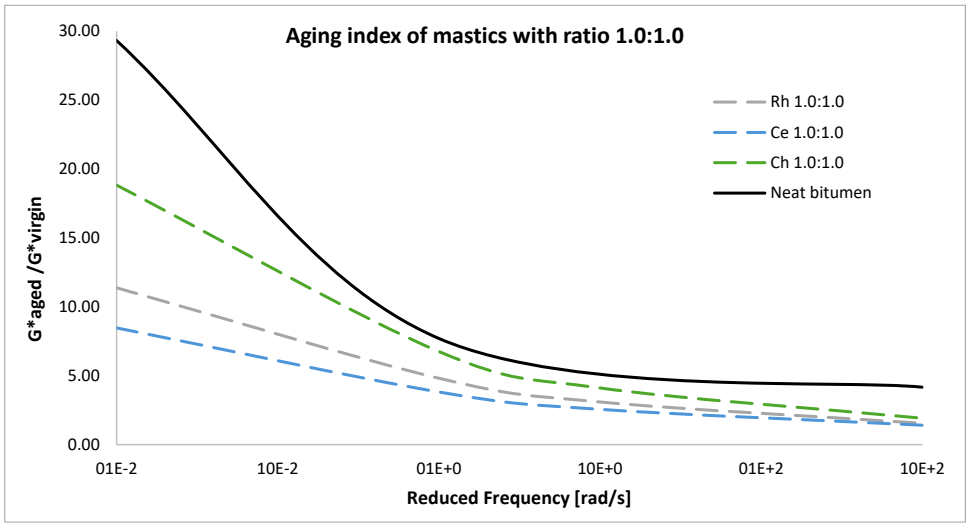

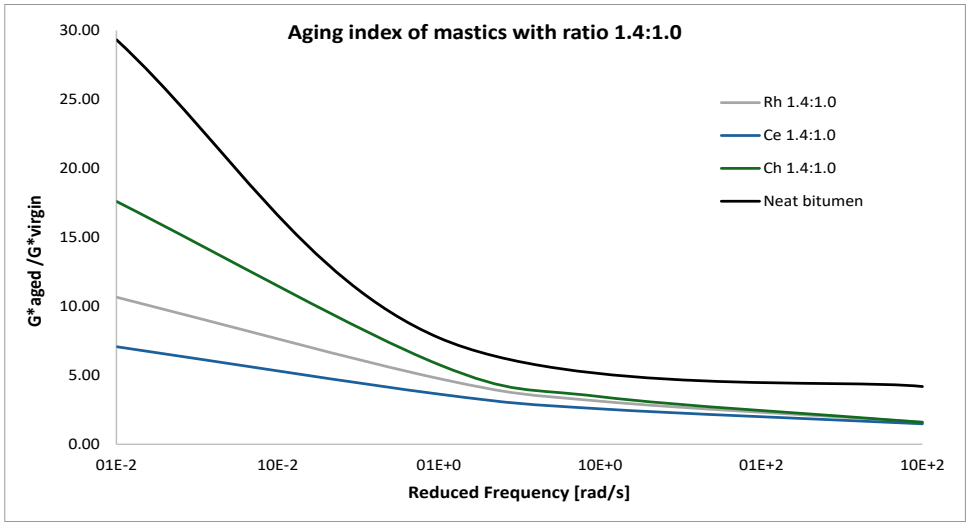

Figure 17 – Aging index of mastics with different filler-to-bitumen ratios

This specific behavioral difference is primarily attributed to the inherent physical properties of the chromium steel sludge. Unlike standard mineral fillers, the chromium steel particles possess a significantly higher thermal conductivity. During the high-temperature conditioning of the long-term aging process, this elevated thermal conductivity facilitates a more rapid and efficient transfer of heat throughout the mastic matrix. Consequently, the bituminous binder surrounding the chromium particles experiences more intense thermal exposure, which slightly accelerates the oxidative reactions and results in a stiffer aged mastic compared to those containing the more thermally insulating traditional fillers.

4.3 Self-Healing Assessment

4.3.1 Selection of Fatigue Parameters

Before initiating the self-healing protocol, preliminary Amplitude Sweep tests were conducted on six mastic (ratios of 0.6 and 1.0) to precisely define the appropriate damage conditions. The primary objective of this preliminary testing was to identify a specific strain level and testing temperature that would successfully induce measurable internal micro-damage without causing catastrophic, macroscopic failure of the specimen.

The selection of these critical parameters was based on a fundamental rheological trade-off. If the applied strain is too low or the testing temperature is too high, the material remains entirely within its LVE region; under these specific conditions, no internal structural damage occurs, making it impossible to evaluate any subsequent healing capabilities. Conversely, if the applied strain is too high or the testing temperature is too low, the internal structure of the specimen is completely destroyed, leading to macroscopic failure and rendering any structural recovery impossible.

Based on the results obtained from the amplitude sweep tests, a testing temperature of 20 °C and a constant strain amplitude of 2% were selected as the optimal common parameters for all the evaluated mastics. As illustrated in the Figure 18, applying a 2% strain at 20 °C ensured that all the mastics had safely surpassed their LVE limit, the initial region where the complex shear modulus remains constant, and successfully entered the intended damage zone. Crucially, at this precise strain level, the materials had not yet reached their flow point where the complex modulus drops toward zero, ensuring the structural integrity was compromised just enough to accurately measure the subsequent self-healing recovery.

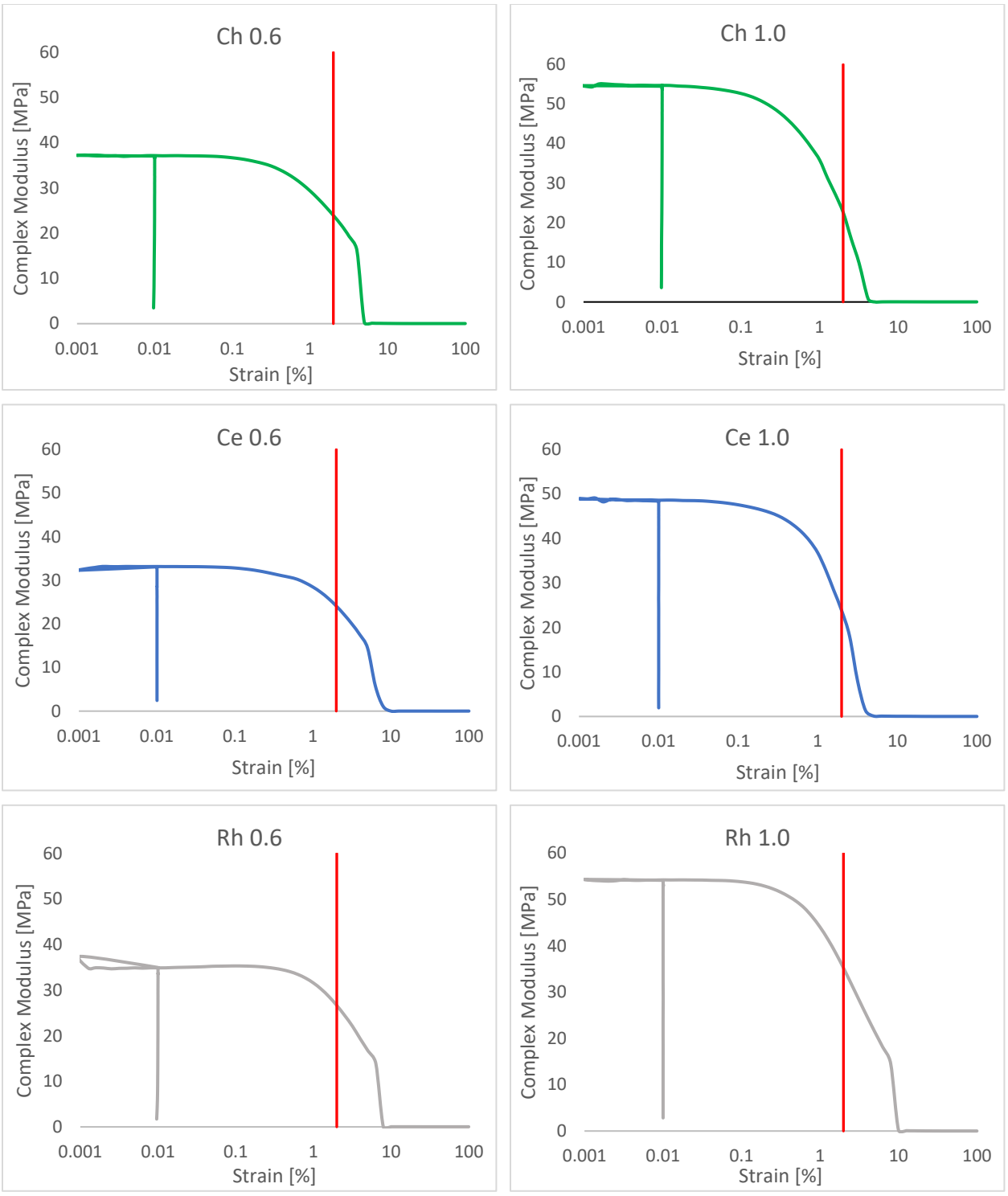

Figure 18 – Determination of strain level and temperature for fatigue tests

4.3.2 Stiffness Recovery (I_G)

To ensure the statistical reliability of the self-healing assessment, multiple testing repetitions were performed for each mastic configuration at the specific filler-to-binder ratios of 0.6 and 1.0. Following the data collection, a rigorous statistical analysis was applied to identify any potential anomalies. Outliers were detected using the Grubbs test at a 95% confidence level, and any values exceeding the critical statistical threshold were carefully excluded only when a clear experimental justification was available. The finalized results for the stiffness recovery index (I_G) are presented in the Figure 19.

Based on these experimental findings, a clear behavioral distinction was observed among the evaluated materials. The reference Rheofiller exhibited the highest overall stiffness recovery at the lower filler concentration; however, as its filler-to-binder ratio was incrementally increased to 1.0, a distinct downward trend in healing capacity was noted. In contrast, the ordinary Portland cement displayed an inverse healing progression. While its initial recovery was lower than that of the Rheofiller, the healing capacity of the cement mastic improved significantly as the filler content was increased. This positive trend suggests that the specific presence and dispersion of the cement particles do not fundamentally hinder the necessary flow of the bitumen required to successfully repair the internally induced micro-cracks.

Conversely, the mastics formulated with the chromium steel sludge recorded the lowest stiffness recovery values across all the evaluated samples. Interestingly, unlike the conventional fillers, the healing performance of this industrial by-product remained virtually constant, showing almost no change as the filler concentration was increased. This notably reduced and stagnant self-healing performance is directly attributable to the physical packing properties of the dry powder, specifically tying back to the rigden voids results discussed previously. Because the chromium sludge possesses a highly elevated inter-particle void content, it fundamentally absorbs a significantly larger volume of the neat binder to properly coat its surface and fill its internal structure. Consequently, a much lower volume of "free bitumen" remains available within the mastic matrix to effectively mobilize, flow, and physically close the internal micro-cracks during the designated rest period.

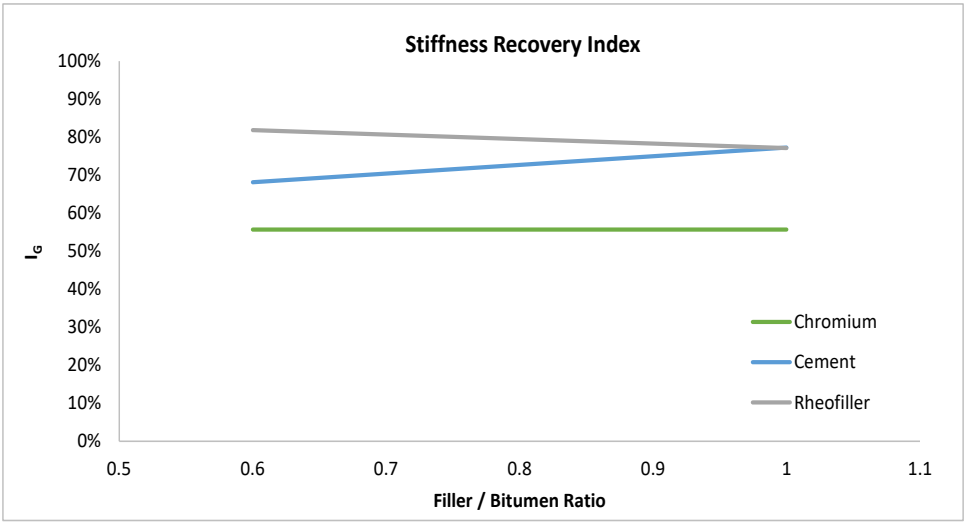

Figure 19 – Stiffness recovery index of the three mastics

4.3.3 Fatigue Endurance (I_N)

Along with stiffness recovery, the healing ability of the mastics was evaluated using the fatigue endurance index (I_N). This index measures how much the material's fatigue life is actually extended after it is given a rest period. To make sure the data was completely reliable, also for I_N an outlier check was performed specifically on these cycle counts. The Grubbs test was applied at a 95% confidence level to both the N_{FRF} and N_{RF} results, which allowed any unusual data points to be carefully identified and removed.

Once the data was finalized for the 0.6 and 1.0 filler-to-binder ratios, a clear pattern emerged. Interestingly, as it is shown in the Figure 20, the fatigue endurance results showed a completely different trend compared to the stiffness recovery we looked at earlier. For all the tested mastics, adding more filler consistently led to a noticeable improvement in the fatigue endurance index. This universal increase shows that having a higher concentration of solid particles within the mastic actually helps to prolong the material's overall fatigue life after a healing phase.

When looking at the specific materials, the mastics made with the chromium steel sludge showed the best overall performance for fatigue endurance. Even though the chromium mastic was the worst at recovering its initial stiffness, it provided the greatest relative extension in fatigue life. This ability was enhanced even further as more chromium was added to the mix.

The excellent fatigue endurance of the chromium mastic points to an interesting interaction between the industrial particles and the bitumen. As established earlier, the high Rigden voids of the chromium sludge restrict the flow of the "free bitumen," making it hard for the material to quickly seal micro-cracks and regain its original stiffness. However, the dense packing of these rigid particles seems to act like a strong internal reinforcement. Once the rest period is over and the testing loads resume, these tightly packed particles likely help bridge the tiny internal cracks and absorb the mechanical stress.

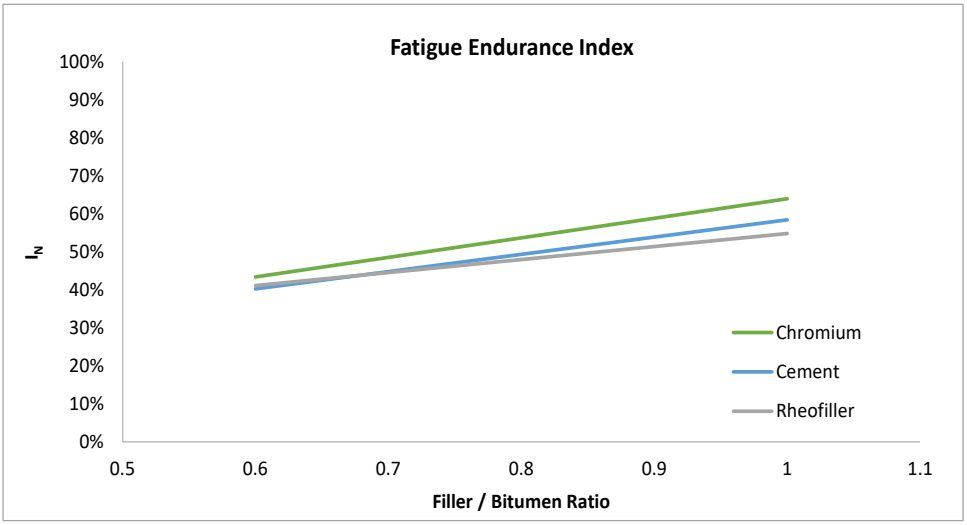

Figure 20 – Fatigue endurance index of the three mastics

Chapter 5: Conclusions

This study was conducted to evaluate the feasibility of utilizing chromium steel sludge, an industrial by-product, as a sustainable alternative filler in bituminous mastics. Through a comprehensive laboratory investigation, its physical, rheological, aging, and self-healing properties were assessed and directly compared against traditional mineral fillers, specifically Rheofiller and ordinary Portland cement. Based on the experimental results and analyses, the following main conclusions can be drawn:

- Physical Characteristics and Volumetric Design: The chromium steel sludge exhibits a significantly higher particle density (5.91 Mg/m^3) compared to standard fillers (2.72 Mg/m^3 for Rheofiller and 3.1 Mg/m^3 for cement). Furthermore, it presents a remarkably high Rigden void content of 59.0%, indicating highly irregular particle shapes and poor packing efficiency. These characteristics mandate a volumetric mix design, as the high void content absorbs a substantial amount of "fixed bitumen," reducing the volume of "free bitumen" available for lubrication and flow.
- Unaged Rheological Performance: Increasing the filler-to-binder ratio consistently increases the complex shear modulus (G^*) across all mastic types, confirming that structural stiffening is primarily governed by volumetric concentration. At high filler concentrations (ratio of 1.4), the specific mineralogy plays a more prominent role. Under these conditions, the chromium mastic proved highly advantageous, exhibiting lower stiffness at low temperatures (enhancing thermal cracking resistance) and higher stiffness at elevated temperatures (enhancing rutting resistance) compared to traditional fillers.

- Aging Susceptibility: The inclusion of all tested mineral fillers successfully mitigated the oxidative aging of the neat bitumen by creating a physical barrier that restricts oxygen diffusion. Furthermore, for all mastics, increasing the filler-to-binder ratio from 0.6 to 1.4 further decreased the aging index. However, when compared to standard fillers, the chromium mastic exhibited a slightly higher aging index. This vulnerability is attributed to the inherently higher thermal conductivity of the chromium steel particles, which facilitates rapid heat transfer and accelerates internal thermal degradation during long-term exposure.
- Self-Healing and Fatigue Endurance: The high Rigden void content of the chromium sludge significantly hinders its stiffness recovery (I_G). The lack of mobile "free bitumen" makes it difficult for the mastic to physically flow and seal internal micro-cracks during rest periods, resulting in the lowest I_G values among the evaluated mastics. Conversely, the chromium mastic demonstrated the highest Fatigue Endurance Index (I_N). The dense packing of these rigid particles acts as robust internal reinforcement, effectively bridging internal cracks upon reloading and significantly extending the material's fatigue life after a healing phase.

Final Verdict: Overall, chromium steel sludge demonstrates significant potential as a sustainable alternative filler for road paving applications. While its high density and elevated Rigden voids present challenges regarding stiffness recovery and require careful volumetric mix design, its excellent performance in extending fatigue life and resisting high-temperature rutting makes it a highly valuable material. Its use not only offers acceptable rheological performance but also provides an effective solution for recycling industrial waste within the construction sector.

References

AASHTO - T 391-20. (2021). Standard Method of Test for Estimating Fatigue Resistance of Asphalt Binders Using the Linear Amplitude Sweep.

Airey, G. (2003). Rheological properties of styrene butadiene styrene polymer modified road bitumens⋆. Fuel, 82(14), 1709–1719. https://doi.org/10.1016/S0016-2361(03)00146-7

Asphalt Institute. (2014). Asphalt Mix Design Methods MS2- 7th. Manual Series.

Bhasin, A., Bommavaram, R., Greenfield, M. L., & Little, D. N. (2011). Use of Molecular Dynamics to Investigate Self-Healing Mechanisms in Asphalt Binders. Journal of Materials in Civil Engineering, 23(4), 485–492. https://doi.org/10.1061/(ASCE)MT.1943-5533.0000200

Bi, Y., Guo, F., Zhang, J., Pei, J., & Li, R. (2021). Correlation analysis between asphalt binder/asphalt mastic properties and dynamic modulus of asphalt mixture. Construction and Building Materials, 276, 122256. https://doi.org/10.1016/j.conbuildmat.2021.122256

BS EN 1097-4. (2008). Tests for mechanical and physical properties of aggregates Part 4: Determination of the voids of dry compacted filler.

BS EN 1097-7. (2022). Tests for mechanical and physical properties of aggregates Part 7: Determination of the particle density of filler—Pyknometer method.

BS EN 14769. (2023). Bitumen and bituminous binders—Accelerated long-term ageing conditioning by a Pressure Ageing Vessel (PAV).

BS EN 14770. (2012). Bitumen and bituminous binders—Determination of complex shear modulus and phase angle—Dynamic Shear Rheometer (DSR).

Camargo, I. G. D. N., Hofko, B., Mirwald, J., & Grothe, H. (2020). Effect of Thermal and Oxidative Aging on Asphalt Binders Rheology and Chemical Composition. Materials, 13(19), 4438. https://doi.org/10.3390/ma13194438

Carvajal-Muñoz, J. S., & Airey, G. (2025). A micromechanics-rheological approach to study the stiffening mechanism of hydrated lime in asphalt mastics. Road Materials and Pavement Design, 1–32. https://doi.org/10.1080/14680629.2025.2543900

Chen, M., Javilla, B., Hong, W., Pan, C., Riara, M., Mo, L., & Guo, M. (2019). Rheological and Interaction Analysis of Asphalt Binder, Mastic and Mortar. Materials, 12(1), 128. https://doi.org/10.3390/ma12010128

Christensen, D. W., & Anderson, D. A. (1992). Interpretation of dynamic mechanical test data for paving grade asphalt cements (with discussion). Journal of the Association of Asphalt Paving Technologists, 61.

Dadaei, M. M., Hajikarimi, P., Esfandiar, M., Rahi, M., Dastoori Razaz, M., Tahmasbi, B., & Moghadas Nejad, F. (2024). Investigation on the Effect of Long-Term Aging on Low-Temperature Viscoelastic Behavior of Bitumen through Physicochemical Characterization. Journal of Materials in Civil Engineering, 36(5), 04024068. https://doi.org/10.1061/JMCEE7.MTENG-16949

EN 197-1. (2011). Cement – Part 1: Composition, specifications and conformity criteria for common cements.

EN 12591. (2009). Bitumen and bituminous binders – Specifications for paving grade bitumens.

EN 13043. (2002). Aggregates for bituminous mixtures and surface treatments for roads, airfields and other trafficked areas.

Faheem, A. F., & Bahia, H. U. (2010). Modelling of Asphalt Mastic in Terms of Filler-Bitumen Interaction. Road Materials and Pavement Design, 11(sup1), 281–303. https://doi.org/10.1080/14680629.2010.9690335

Hou, J., Ma, X., Chen, H., & Wang, Z. (2022). A comparison of indices used to evaluate asphalt-filler interactions. Construction and Building Materials, 359, 129501. https://doi.org/10.1016/j.conbuildmat.2022.129501

Hou, Y., Wang, L., Pauli, T., & Sun, W. (2015). Investigation of the Asphalt Self-Healing Mechanism Using a Phase-Field Model. Journal of Materials in Civil Engineering, 27(3), 04014118. https://doi.org/10.1061/(ASCE)MT.1943-5533.0001047

Kim, Y. R., Little, D. N., Benson, F. C., & Assoc, J. (1990). Asphalt Paving Technol (Vol. 59).

Kim, Y.-R., & Little, D. N. (2004). Linear Viscoelastic Analysis of Asphalt Mastics. Journal of Materials in Civil Engineering, 16(2), 122–132. https://doi.org/10.1061/(ASCE)0899-1561(2004)16:2(122)

Lesueur, D., Teixeira, A., Lázaro, M. M., Andaluz, D., & Ruiz, A. (2016). A simple test method in order to assess the effect of mineral fillers on bitumen ageing. Construction and Building Materials, 117, 182–189. https://doi.org/10.1016/j.conbuildmat.2016.05.003

Li, C., Wu, S., Tao, G., & Xiao, Y. (2018). Initial Self-Healing Temperatures of Asphalt Mastics Based on Flow Behavior Index. Materials, 11(6), 917. https://doi.org/10.3390/ma11060917

Li, H., Jiang, J., Li, S., & Ma, X. (2019). Evaluation of the Rheological Property of Binder-Filler Systems after Oxidation Based on a Simple Film Oven Aging Method. Applied Sciences, 9(12), 2542. https://doi.org/10.3390/app9122542

Li, S., Ni, F., Dong, Q., Zhao, Z., & Ma, X. (2021). Effect of filler in asphalt mastic on rheological behaviour and susceptibility to rutting. International Journal of Pavement Engineering, 22(1), 87–96. https://doi.org/10.1080/10298436.2019.1577423

Li, X., Liu, Z., Fu, K., Zhang, K., & Chen, M. (2026). Composition optimization of mastic in recycled asphalt mixtures based on pavement performance. PLOS One, 21(3), e0344180. https://doi.org/10.1371/journal.pone.0344180

Miglietta, F., Tsantilis, L., Baglieri, O., & Santagata, E. (2021). A new approach for the evaluation of time–temperature superposition effects on the self-healing of bituminous binders. Construction and Building Materials, 287, 122987. https://doi.org/10.1016/j.conbuildmat.2021.122987

Migliori, F., & Corté, J.-F. (1998). Comparative Study of RTFOT and PAV Aging Simulation Laboratory Tests. Transportation Research Record: Journal of the Transportation Research Board, 1638(1), 56–63. https://doi.org/10.3141/1638-07

Riccardi, C., Cannone Falchetto, A., Losa, M., & Wistuba, M. P. (2018). Development of simple relationship between asphalt binder and mastic based on rheological tests. Road Materials and Pavement Design, 19(1), 18–35. https://doi.org/10.1080/14680629.2016.1230514

Salehfard, R., Yeganeh, S., Dalmazzo, D., Underwood, B. S., & Santagata, E. (2024). Linking Chemical Structure to the Linear and Nonlinear Properties of Asphalt Binders. Transportation Research Record: Journal of the Transportation Research Board, 2678(11), 1483–1495. https://doi.org/10.1177/03611981241244793

Santagata, E., Miglietta, F., Baglieri, O., & Tsantilis, L. (2022). Effect of Temperature on Self-healing Properties of Bituminous Binders. In H. Di Benedetto, H. Baaj, E. Chailleux, G. Tebaldi, C. Sauzéat, & S. Mangiafico (Eds.), Proceedings of the RILEM International Symposium on Bituminous Materials (Vol. 27, pp. 623–629). Springer International Publishing. https://doi.org/10.1007/978-3-030-46455-4_79

Tan, Y., & Guo, M. (2013). Study on the phase behavior of asphalt mastic. Construction and Building Materials, 47, 311–317. https://doi.org/10.1016/j.conbuildmat.2013.05.064

Williams, D., Lytton, R. L., Little, D. N., Kim, Y., & Kim, Y. R. (2001). Microdamage Healing in Asphalt and Asphalt Concrete, Volume 2: Laboratory and Field Testing to Assess and Evaluate Microdamage and Microdamage Healing (Vol. 2).

Wu, J., & Airey, G. (2011). The Influence of Mineral Fillers on Mastic Aging Properties. ICCTP 2011, 3450–3461. https://doi.org/10.1061/41186(421)342

Xie, X., Li, H., Duan, J., Li, G., & Tong, S. (2020). Influence of the Mineral Powder Content on the Asphalt Aging Resistance in High-Altitude Areas Based on Indoor Ultraviolet Light Tests. Materials, 13(3), 754. https://doi.org/10.3390/ma13030754

Xing, C., Liu, L., & Sheng, J. (2020). A new progressed mastic aging method and effect of fillers on SBS modified bitumen aging. Construction and Building Materials, 238, 117732. https://doi.org/10.1016/j.conbuildmat.2019.117732

Xu, S., García, A., Su, J., Liu, Q., Tabaković, A., & Schlangen, E. (2018). Self-Healing Asphalt Review: From Idea to Practice. Advanced Materials Interfaces, 5(17), 1800536. https://doi.org/10.1002/admi.201800536

Yeganeh, S., Ameri, M., Dalmazzo, D., & Santagata, E. (2020). Experimental Investigation on the Use of Waste Elastomeric Polymers for Bitumen Modification. Applied Sciences, 10(8), 2671. https://doi.org/10.3390/app10082671

Zheng, C., Li, R., Zou, L., Lv, D., & Xu, Y. (2018). Effects of Filler–Bitumen Ratio and Mineral Filler Characteristics on the Low-Temperature Performance of Bitumen Mastics. Materials, 11(7), 1155. https://doi.org/10.3390/ma11071155